H₄octox: Versatile Bimodal Octadentate Acyclic Chelating Ligand for Medicinal Inorganic Chemistry

Xiaozhu Wang,[†] María de Guadalupe Jaraquemada-Peláez,[†] Cristina Rodríguez-Rodríguez,[‡,§] Yang Cao,[†] Christian Buchwalder,[∥] Neha Choudhary,[†,⊥] Una Jermilova,[†,⊥] Caterina F. Ramogida,[⊥,#] Katayoun Saatchi,[∥] Urs O. Häfeli,[∥] Brian O. Patrick,[†] and Chris Orvig*,[†]

[†]Medicinal Inorganic Chemistry Group, Department of Chemistry, University of British Columbia, 2036 Main Mall, Vancouver, British Columbia V6T 1Z1, Canada

[‡]Center for Comparative Medicine, 4145 Wesbrook Mall, Vancouver, British Columbia V6T 1W5, Canada

[§]Department of Physics and Astronomy, University of British Columbia, 6224 Agronomy Road, Vancouver, British Columbia V6T 1Z1, Canada

[∥]Faculty of Pharmaceutical Sciences, University of British Columbia, 2405 Wesbrook Mall, Vancouver, British Columbia V6T 1Z3, Canada

[⊥]Life Sciences Division, TRIUMF, 4004 Wesbrook Mall, Vancouver, British Columbia V6T 2A3, Canada

[#]Department of Chemistry, Simon Fraser University, 8888 University Drive, Burnaby, British Columbia V5A 1S6, Canada

ⓢ *Supporting Information*

ABSTRACT: H₄octox, a versatile new octadentate acyclic chelating ligand, has been investigated as an alternative to the acyclic DTPA and the macrocyclic DOTA for trivalent metal ions useful in diagnostic medical imaging or therapeutic applications (Y^{3+}, In^{3+}, La^{3+}, Gd^{3+}, Lu^{3+}). The synthesis of H₄octox is straightforward in less steps and thus more economical than those of most previously reported chelators. Complex formation equilibria in the presence of Y^{3+}, In^{3+}, La^{3+}, Gd^{3+}, and Lu^{3+} revealed fast chelation and high metal-sequestering capacity. Quantitative labeling with $^{111}In^{3+}$ was achieved within 15 min at room temperature at ligand concentrations as low as 10^{-7} M, exactly the properties required for the development of kit-based radiopharmaceuticals. *In vitro* serum stability studies and *in vivo* SPECT imaging confirmed excellent complex stability of [^{111}In-(octox)]⁻. Moreover, it is more lipophilic than most of the multidentate carboxylate- or picolinate-based chelators; it therefore shows more liver clearance and provides a complementary choice in the design of metal-based pharmaceuticals and in the tuning of their pharmacokinetic properties. Finally, H₄octox showed a large fluorescence enhancement upon complexation with different metals, in particular, with Y^{3+} and Lu^{3+}, which could be useful for non-radioactive fluorescent stability and cell studies as well as bimodal imaging. Excellent *in vitro* stability of [Y(octox)]⁻ against transferrin and Fe^{3+} was confirmed employing this fluorescence.
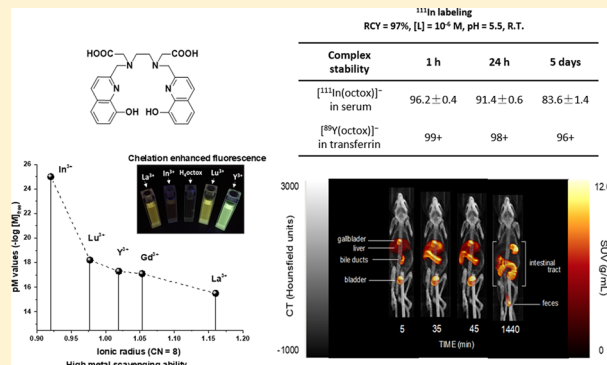
INTRODUCTION

^{111}In is an important cyclotron-produced isotope in nuclear medicine. The long half-life of ^{111}In (2.8 days) matches biovectors with a long biological half-life, such as antibodies.[1] It decays by electron capture with emission of γ rays (245 and 172 keV), that can be used for single-photon emission-computed tomography (SPECT) imaging, and Auger electrons, which can be used for therapy.[2] ^{110m}In ($t_{1/2}$ = 69 min) has also attracted interest because of its potential application in positron emission tomography (PET) imaging.[3]

^{177}Lu ($t_{1/2}$ = 6.6 days, 134.17 keV) and ^{90}Y ($t_{1/2}$ = 2.67 days, 933.61 keV) are two important β⁻ emission radioisotopes used in therapy. ^{90}Y only emits β⁻ particles and is therefore usually

used in combination with ^{111}In as a congener for imaging and dosimetry, based on the same charge and similar size of their metal ions.[2,4−6]

The application of all of these metal ions and isotopes mentioned above and their combined or interchanged use requires a good chelator that can bind them with high thermodynamic stability and kinetic inertness. DTPA (diethylenetriamine pentaacetic acid) and DOTA (1,4,7,10-tetraazacyclododecane-1,4,7,10-tetraacetic acid) are the most commonly used chelators in recent years.[1] DTPA is an acyclic

chelator which can radiolabel these metal ions fast (within 15 min) at mild conditions (ambient temperature) and is used in currently available FDA-approved ^{111}In-based radiopharmaceuticals; however, it shows inferior *in vivo* stability compared to the macrocyclic chelator DOTA.[7,8] This is a large limitation for the therapeutic radiopharmaceuticals which require a high dose. For example, unstable ^{90}Y-DTPA complexes cause bone accumulation of free ^{90}Y, of which even a small amount can contribute significantly to bone marrow toxicity due to long-range β-particles. Thus, the maximum tolerated dose of ^{90}Y-DTPA-mABs (e.g., zevalin) is 32 mCi, much lower than the 150 mCi safely administered of ^{131}I-labeled mABs.[9−11] In addition, Gd-DTPA was recently removed from the European market due to brain Gd^{3+} retention, which adds to the urgency of finding more stable alternatives in the radiopharmaceutical arena as well.[12] DOTA, on the other hand, requires elevated temperatures (60−95 °C) and extended reaction times (30−120 min) to achieve quantitative radiolabeling yields and is not suitable for thermally sensitive carriers such as antibodies.[13,14]

Significant effort has been made in the past decade to overcome these limitations. A summary of the most representative chelators is presented in Scheme 1.[13−19] For

Scheme 1. Representative Chelating Ligands for In^{3+}, Y^{3+}, Lu^{3+}, and Gd^{3+} in the Literature
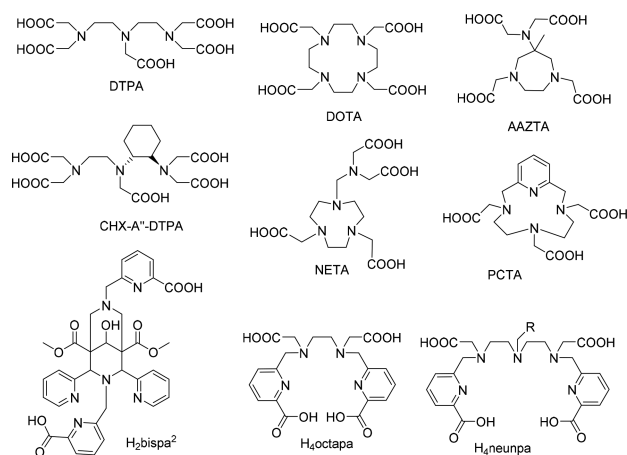
macrocyclic chelators, one major strategy to accelerate the complexation kinetics is to create a hybrid chelator by introducing an acyclic moiety, for example, both AAZTA and NETA added one iminodiacetic acid group to the macrocyclic backbone. CHX-A″-DTPA has a rigid cyclohexane modification and showed increased stability.[8,16,20,21] H$_4$octapa, H$_4$neunpa, and H$_2$bispa^2 exploit the picolinic acid motif, which decreases the flexibility of the chelator.[14,18] There remain limitations. Most of the hybrid chelators show decreased stability compared to DOTA, and the reinforced acyclic chelator CHX-A″-DTPA still shows clear dissociation *in vivo*. The syntheses of these molecules are often quite complex and time consuming, and thus they have limited application. Most of them are also quite hydrophilic and will accelerate the renal clearance of the pharmaceuticals especially when the carrier is small.

Herein, we report an octadentate chelator, H$_4$octox, the design of which was inspired by H$_4$octapa and In(oxine)$_3$, which has been used in white blood cell labeling for 30 years (Scheme 2).[22] The synthesis of this new chelator is significantly easier and cheaper than for most previously

reported chelators. H$_4$octox shows fast chelation with metal ions (Y^{3+}, In^{3+}, La^{3+}, Lu^{3+}, and Gd^{3+}) and forms highly stable complexes in solution. The *in vivo* stability was confirmed with ^{111}In SPECT imaging. Moreover, H$_4$octox, compared with the multiarmed carboxylic or picolinic acid-based chelators in Scheme 1, is more lipophilic and therefore shows a longer circulation time and more liver clearance. Another distinguishing property is its enhanced fluorescence once chelated with Y^{3+} and Lu^{3+}—potentially useful for bimodal imaging.

■ RESULTS AND DISCUSSION

Synthesis and Characterization. The simple bidentate ligand 8-hydroxyquinoline (oxine) has proven to have a high affinity for In^{3+}; ^{111}In(oxine)$_3$ has been used in white blood cell labeling for 30 years. Therefore, 8-hydroxyquinoline could be a really suitable motif upon which to build larger multidentate chelator platforms. H$_4$octapa[14] has shown excellent *in vitro* and *in vivo* stability with In^{3+}, and its bifunctional derivative showed even better performance than DOTA and DTPA. By combining the geometry of H$_4$octapa and the rigid 8-hydroxyquinoline motif for "arms", we designed H$_4$octox as shown in Scheme 2.

**Scheme 2. Design Paradigm for H$_4$octox**
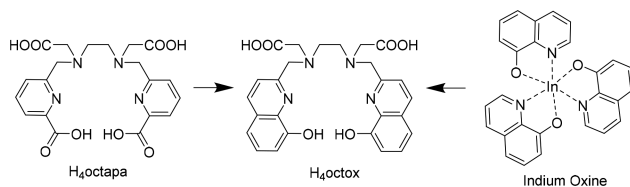
In the synthesis of H$_4$octox (Scheme 3), the precursor H$_2$hox (**1**) was synthesized first as we have reported[23] and then conjugated with *tert*-butyl bromoacetate. The protection of the phenol group was not needed in this step, since the electrophilicity of the secondary amine backbone is higher than that of the phenol oxygen in the 8-hydroxyquinoline. The HCl salt of H$_4$octox was finally obtained by deprotection of *tert*-butyl ester groups using 6 M HCl. The final product was characterized by ^{1}H and ^{13}C NMR spectroscopy and its purity confirmed by elemental analysis.

Scheme 3. Synthesis of H$_4$octox^a
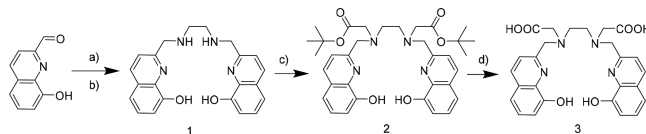
^{a}Reagents and conditions: (a) en, CH$_3$CH$_2$OH, 60 °C, 4 h; (b) CH$_3$CH$_2$OH, NaBH$_4$ overnight, 91%; (c) CH$_3$CN, *tert*-butyl bromoacetate, NaHCO$_3$ (excess), 50 °C, 24 h, 84%; (d) HCl (6 M), 60 °C, overnight, 97%.

The whole synthetic route is straightforward, and the cumulative yield (74%) is higher than that for any of H$_4$octapa, H$_4$neunpa, and most of the other chelators in Scheme 1. The use of multiple synthons is also an advantage for a straightforward preparation of bifunctional derivatives using a functionalized diamine backbone (for example, (4-nitro-benzyl)-ethylenediamine) compared with the tedious synthesis of certain bifunctional macrocyclic chelators. The good
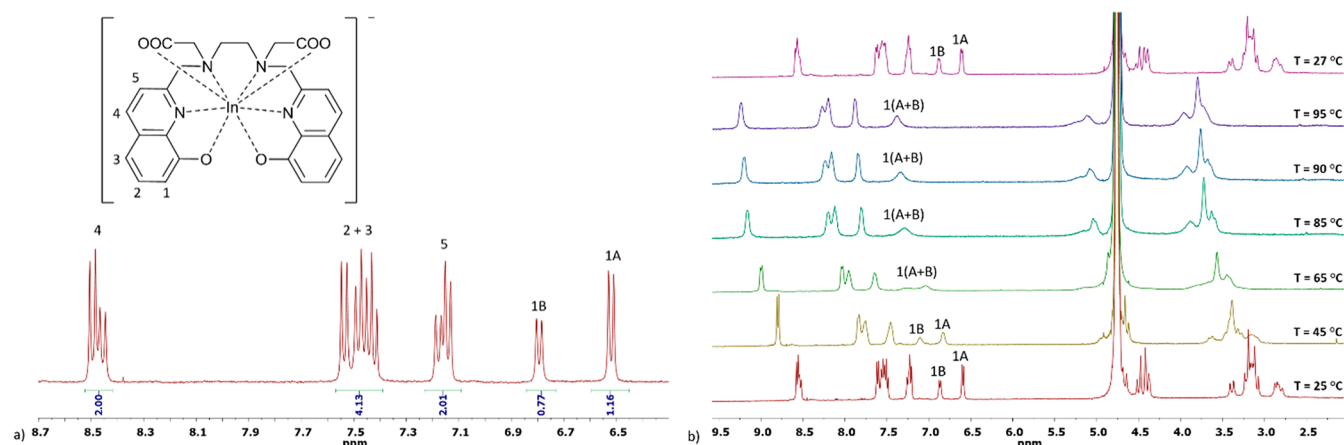
Figure 1. (a) Portions of the ^{1}H NMR spectra of $[In(octox)]^-$ in D_2O showing the aromatic protons (pH = 8, 400 MHz, 25 °C). (b) VT ^{1}H NMR experiment for $[In(octox)]^-$ (pH = 8, 400 MHz). A and B represent the two different species in solution of the $[In(octox)]^-$ complex.

synthetic accessibility together with the low cost of the starting materials easily available from commercial suppliers is of great importance for wide uptake, application, and clinical use.

$[In(octox)]^-$ was prepared by directly mixing the HCl salt of H_4octox with $In(ClO_4)_3$ in H_2O in an equimolar ratio and adjusting the pH to 8 with NaOH. Metal complexation of H_4octox with In^{3+} was confirmed by ^{1}H NMR spectroscopy (Figure 1), and a fully 8-coordinated solution structure of $[In(octox)]^-$ is suggested from the sharp resolved diastereotopic splitting of the protons associated with all six methylene $-CH_2$ protons in H_4octox (Figure S14). Two distinct symmetrical isomeric species are present in solution at pH 8 based on the integration of the well-resolved aromatic proton signals (1A and 1B) in Figure 1a. The existence and exchange of the two possible isomers was further evidenced by VT-NMR and NOESY experiments (Figures 1b and S16). At room temperature, the exchange is slow on the NMR time scale, so two different sets of signals are observed, and when the temperature is raised (Figure 1b), the exchange between the two isomers is faster and two peaks (1A and 1B) merged into one broad peak (1(A + B)); similar changes can be observed for the rest of the signals. NOESY experiments at room temperature showed exchange between the two sets of peaks within both the aromatic and the aliphatic protons. The expected NOE within aromatic protons between protons 1 and 2, and 2 and 3, as well as 4 and 5, for both isomers were observed; however, no NOE was observed between aliphatic protons due to a small T1 for those protons and the relatively low concentration (Figure S16).

X-ray Crystallography. The structure of the $[La(octox)]^-$ complex is not of very high quality due to the poor quality of the crystals, and the cation(s) not identified, but the coordination environment of the La(III) ion is perfectly clear. In spite of several attempts using different disorder models, the refinement of the co-crystallized solvent molecules and cations remained unstable. The solvent regions could not be reasonably modeled; therefore, the PLATON/SQUEEZE[24] program was employed to generate "solvent-free" data. The structure details can be found in the Supporting Information (Figure S17). Selected average bond distances and angles are shown in Table 1. In Figure 2, it can be seen that La3 is 10-coordinated: the coordination sphere consists of eight donor atoms (N_4O_4) from $octox^{4-}$, one O-atom (O18) from the

Table 1. Selected Average Bond Angles and Bond Distances in the $[La(octox)]^-$ Complex

|	
(ox-N)N–M (Å)	2.708(7)
(en-N)N–M (Å)	2.726(7)
(ox-O)O–M (Å)	2.585(6)
(Ac-CO₂)O–M (Å)	2.556(6)
(Aqua)O–M (Å)	2.560(6)
(ox-N)N–M–(ox-N)N angle (deg)	172.0(2)
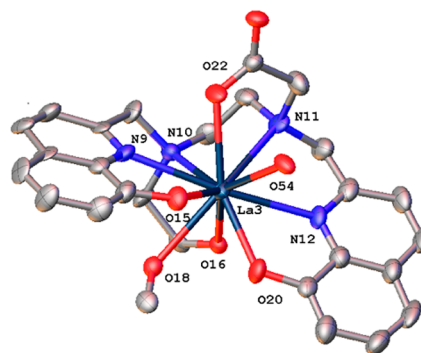
Figure 2. ORTEP diagram of $La[(octox)]^-$ in the asymmetric unit (50% probability ellipsoids). Solvent molecules, cations, and hydrogens are omitted for clarity.

–COOH group from another $octox^{4-}$ molecule, and one molecule of water.

There is a lack of a clear and well-defined geometry around lanthanum center—often the case with non-rigid lanthanide complexes. Nevertheless, this crude crystal structure for $[La(octox)]^-$ provides a visually compelling insight into the nature of the interaction between a trivalent metal ion and the octadentate $octox^{4-}$ motif.

DFT Simulations and Molecular Electrostatic Potential Maps. DFT calculations were carried out to simulate the behavior of the anion $[In(octox)]^-$ in solution. Two most stable isomeric structures A and B were identified featuring different bond conformations of the en backbone (Figure 3). Both structures have 8-coordinated metal centers and exhibit similar C_{2v}-like symmetry and calculated dipole moments. Structure A with equatorial hydroxyquinoline arms is only 8.7 kJ/mol less stable than structure B with axial hydroquinoline groups. These results are consistent with the observations in
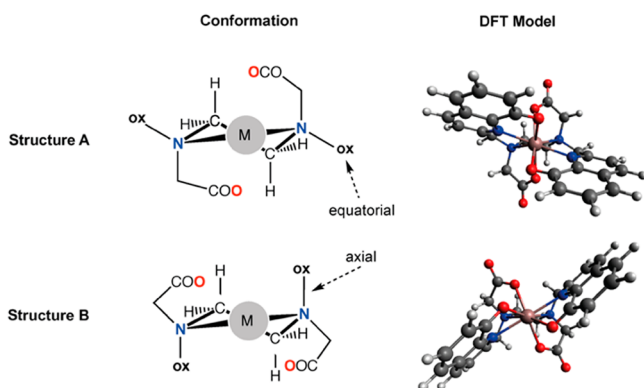
Figure 3. Ball-and-stick presentation of the two isomeric species simulated using DFT calculations.

the ^{1}H NMR solution study of $[In(octox)]^-$ in which two coexisting isomers were found to have different coupling patterns in the aliphatic region. Similar isomers have also been identified in the $[In(octapa)]^-$ anion,[14] and the corresponding structure A is 6.4 kJ/mol less stable than structure B. These isomers were not observed in $[In(octapa)]^-$ possibly due to a much faster equilibrium between isomers resulting from the somewhat less rigid ligand structure in octapa; therefore, only the averaged signal was observed.[14]

$[In(octox)]^-$ and $[In(octapa)]^-$ have been compared by examining the calculated structures and electrostatic potentials. As shown in Table 2, $[In(octapa)]^-$ shows areas of much higher electronegative potential around the picolinic acid group compared to the region of the hydroxyquinoline groups in $[In(octox)]^-$. This difference may result in a lower propensity toward protonation and slower decomposition under acidic conditions for $[In(octox)]^-$.
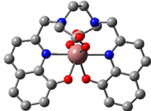
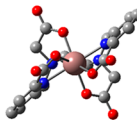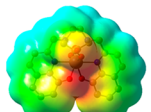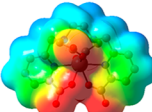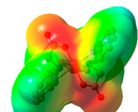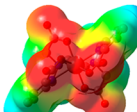**Solution Thermodynamics.** When evaluating metal-chelating ligands for radiopharmaceutical applications, knowledge of their acid–base properties (protonation constants) and the thermodynamic stability of their metal complexes is critical, and in particular, the extent to which a metal complex is formed in solution at physiologically relevant conditions ca. pH 7.4. The most effective thermodynamic comparison of the vast array of metal chelators that have been developed for radiopharmaceutical purposes is via conditional stability constants. The metal-ion-scavenging parameter pM was

introduced by Raymond[25] (defined as $-\log[M_{free}]$ at $[L] = 10\,\mu M$, $[M] = 1\,\mu M$, and pH = 7.4) and gives insight into the stability of the complexes *in vivo*, allowing for the most suitable comparison of the ability of different ligands with diverse basicities and protonation states to sequester specific metal ions. Values of pM are linearly correlated to the conditional stability constant of metal complexes but, most importantly, depend on the ligand basicity and/or denticities and difference in metal–ligand stoichiometries and thus on the competition of the metal and proton for the same coordinating groups.[26–28]

Recently, our group has reported an exhaustive UV spectrophotometric analysis of the protonation equilibria of H_2hox, a new promising hexadentate Ga^{3+} chelator for PET imaging.[23] In this work we report the eight protonation constants ($\log K$) of the octadentate derivative version of H_2hox, H_4octox. The two additional carboxylic acid substituents in H_4octox confer a higher aqueous solubility than that of H_2hox, allowing the use of the simultaneous UV–potentiometric titrations for the determination of protonation constants. The dissociation of the most acidic protons in H_4octox, species H_8L^{2+} and H_7L^+, respectively, were determined by in-batch UV spectrophotometric titrations as the pH was lower than the electrode threshold. As in the case of H_2hox, the spectral features of H_4octox in the spectral range 200–450 along the titration allowed for the determination and assignment of the protonation events to the different functionalities (Figures S1 and S2). The protonation constants were calculated by using the HypSpec2014[29] program and are summarized in Table 3. Solution speciation diagrams were calculated using the acidity constants given in Table 3 and are shown in Figure S3.

In order to evaluate the affinity of H_4octox toward metal ions of clinical interest—In(III), Y(III), La(III), Gd(III), and Lu(III)—the thermodynamic stability constants of each metal–octox complex have been evaluated by combined UV–potentiometric titrations, and in the case of In(III), due to the high affinity, additional acidic spectrophotometric competitions and ligand–ligand competition potentiometric titrations with the known competitor EDTA were required. In Table 4 are summarized the related stability constants that were refined by using the HypSpec2014 program and in Figures S4–S7 and Figure 4b the related speciation plots.

Table 2. DFT-Optimized Structures and Electrostatic Potential (ESP) Mappings of $[In(octapa)]^-$ and $[In(octox)]^-$ [a]

[a]The ESP mappings represent a maximum potential of 0.03 au and a minimum of −0.20 au mapped onto electron density isosurfaces of 0.002 e·Å^{-3} (red to blue = negative to positive).

Table 3. Protonation Constants of H$_4$octox at 25 °C

equilibrium reaction	log β	log K
L + H$^+$ ⇌ HL	10.65(1)[a]	10.65
HL + H$^+$ ⇌ H$_2$L	20.67(1)[a]	10.02
H$_2$L + H$^+$ ⇌ H$_3$L	29.60(1)[a]	9.03
H$_3$L + H$^+$ ⇌ H$_4$L	34.78(1)[a]	5.18
H$_4$L + H$^+$ ⇌ H$_5$L	37.83(1)[a]	3.05
H$_5$L + H$^+$ ⇌ H$_6$L	39.86(2)[a]	2.03
H$_6$L + H$^+$ ⇌ H$_7$L	39.55(8)[b]	−0.31
H$_7$L + H$^+$ ⇌ H$_8$L	38.88(7)[b]	−0.67

[a]Joined UV−potentiometric titrations at I = 0.16 M NaCl. [b]In-batch UV spectrophotometric titrations, not evaluated at constant I = 0.16 M NaCl. Charges are omitted for clarity.

Combined potentiometric−spectrophotometric titrations of H$_4$octox in with each of Y(III), La(III), Gd(III), and Lu(III) showed the start of the complex formation from pH ≈ 2 based on the distinct features of the spectra compared with the electronic spectra of H$_4$octox (Figures S4−S7) and three consecutive transformations with increasing the pH due to the loss of protons from the species [M(H$_2$L)]$^+$, M(HL), and [M(L)]$^-$, respectively. All of these metal complex deprotonations are marked by the appearance of well-defined isosbestic points (Figures S4−S7). The deprotonations of the neutral species M(HL) may be attributed to the last protonated OH-quinoline moiety, based on the similarity of spectroscopic features to those of [Ga(hox)]$^+$ and Ga(oxine)$_3$ and on its higher basicity compared to that of the −COOH substituents. The last deprotonation is presumably a coordinated water molecule with higher pK_a (10.41−10.81), as previously observed in similar systems.[18,31]

H$_4$octox with In(III) yielded a complete reaction even at pH ≈ 1.6 (spectra in Figures S8a and S8b), and since the determination of thermodynamic stability constants requires the values of the concentration of free and bound metal ions at equilibrium, the direct potentiometric−spectrophotometric method was insufficient and competitive methods were applied to this system, for which the stability constants were determined (Table 4). The system, as with previous metal ions, presented different transformations with pH and [In(H$_2$L)]$^+$, In(HL), [In(L)]$^-$, and [In(OH)(L)]$^{2-}$ species were identified. A particularly high log K = 31.38(1) for the species [In(L)]$^-$ was determined (Table 4). The analysis of Table 5 and Figure 4, in particular the pM values, shows that the size of the metal cation within the cavity of octox^{4-} is best fitted for the smaller and harder metal In^{3+}, and the trend in metal selectivity of this new octadentate acyclic chelator by means of pM value is In^{3+} > Lu^{3+} > Y^{3+} > Gd^{3+} > La^{3+}.
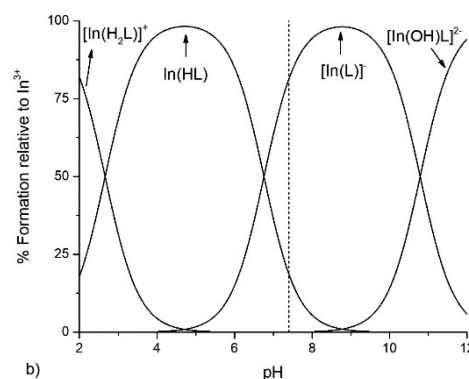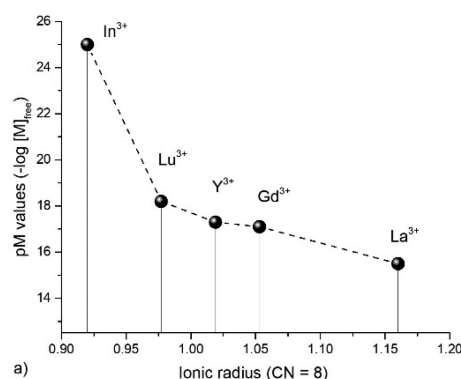

Figure 4. (a) pM values vs ionic radius for M^{3+}−H$_4$octox complexes (CN = 8).[30] (b) Distribution curves for In^{3+}−H$_4$octox complexes, [In^{3+}] = [H$_4$octox] = 8.5 × 10^{-4} M. Dashed line in b at physiological pH (7.4).

In Table 5, the In^{3+} scavenging ability of H$_4$octox, quantified as pIn, is compared to those of the most relevant In^{3+} chelators. The high pIn = 25.0 for the In−octox system, being 6.2 units higher than that of a current gold standard for ^{111}In-based radiopharmaceuticals, DOTA, characterizes H$_4$octox as a promising scaffold for In^{3+} complexation in the development of ^{111}In−BFCs. When comparing the pIn values in Table 5 of the acyclic chelators determined in the past years by our group, only H$_4$octapa exceeds the value of H$_4$octox, by only 1.5 units, because of the higher basicity of H$_4$octox vs H$_4$octapa. Even though the stability constant for [In(octox)]$^-$ (log K_{ML} = 31.38) is higher than that for [In(octapa)]$^-$ (log K_{ML} = 26.8(1)),[14] the competition between the protons and the metal for the basic sites in the ligand is higher in H$_4$octox. Nevertheless, the thermodynamic stability, while a critical parameter for the development of metal-based drugs,

Table 4. Stepwise Stability Constants (log K) of H$_4$octox Complexes with Y^{3+}, La^{3+}, Gd^{3+}, Lu^{3+}, and In^{3+}

equilibrium reaction	Y^{3+} [a]	La^{3+} [a]	Gd^{3+} [a]	Lu^{3+} [a]	In^{3+}
M^{3+} + L ⇌ ML	23.78(3)	21.91(2)	23.54(2)	24.66(1)	31.38(1);[a] 31.64(3)[c]
ML + H$^+$ ⇌ MHL	5.49(3)	6.78(1)	5.96(2)	4.84(2)	6.76(1);[a] 7.08(6)[c]
MHL + H$^+$ ⇌ MH$_2$L	3.71(5)	4.85(2)	4.05(3)	3.51(2)	2.66(1)[b]
M(OH)L + H$^+$ ⇌ ML	10.61(4)	10.81(3)	10.61(4)	10.41(2)	10.69(5);[a] 10.54(4)[c]
pM[d]	17.3	15.5	17.1	18.2	25.0

[a]Combined UV−potentiometric titrations at I = 0.16 M (NaCl) and 25 °C. [b]In-batch acidic spectrophotometric competition at 25 °C; not evaluated at constant I = 0.16 M (NaCl). [c]Ligand−ligand potentiometric competition with EDTA at I = 0.16 M (NaCl) and 25 °C. [d]pM is defined as −log [M]$_{free}$ at [L] = 10 μM, [M] = 1 μM, and pH = 7.4. Charges are omitted for clarity.

Table 5. Comparison of pM^a values for In^{3+} Complexes with H$_4$octox or Literature Chelators

pM	H$_4$octox	H$_4$octapa	H$_4$neunpa	H$_5$decapa	DTPA	CHX-A″-DTPA	DOTA	H$_2$bispa2
pIn^{3+}	25.0	26.5^b	23.6^c	23.1^c	25.7^b	−	18.8^b	25.0^d

^{a}pM = −log [M]$_{free}$ at [L] = 10 μM, [M] = 1 μM, and pH = 7.4. ^{b}From ref 14. ^{c}From ref 18. ^{d}From ref 17.

cannot be considered in isolation, as it does not always correlate well with serum stability or *in vivo* behavior. For example, despite [In(octapa)]$^-$ and [In(DTPA)]$^{2-}$ having higher pIn values than [In(neunpa)]$^-$, it was the latter that showed higher serum stability after 1 day.[18]

Chelation-Enhanced Fluorescence Emission of H$_4$-octox. 8-Hydroxyquinoline shows very weak fluorescence in aqueous solution due to intermolecular photoinduced proton transfer (PPT) between the hydroxyl group and the nearby quinoline nitrogen as well as intermolecular photoinduced electron transfer (PET) from the amine to the hydroxyquinoline moiety. Once complexed with a metal ion (e.g., Zn^{2+}, Mg^{2+}), both PPT and PET are inhibited and the fluorescence intensifies.[32−37] Chelation-enhanced fluorescence (CHEF) emission of the 8-hydroxyquinoline chromophore has been extensively studied and used for the design of fluorescent probes;[38−42] however, it has not yet been reported in radiometal chelating ligands. Herein, we studied the CHEF of H$_4$octox in the presence of Y^{3+}, La^{3+}, Lu^{3+}, and In^{3+}. As shown in Figure 5, at pH 8 in aqueous solution, H$_4$octox
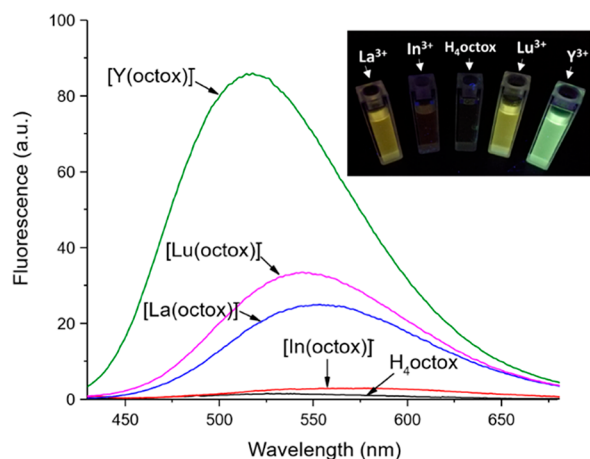
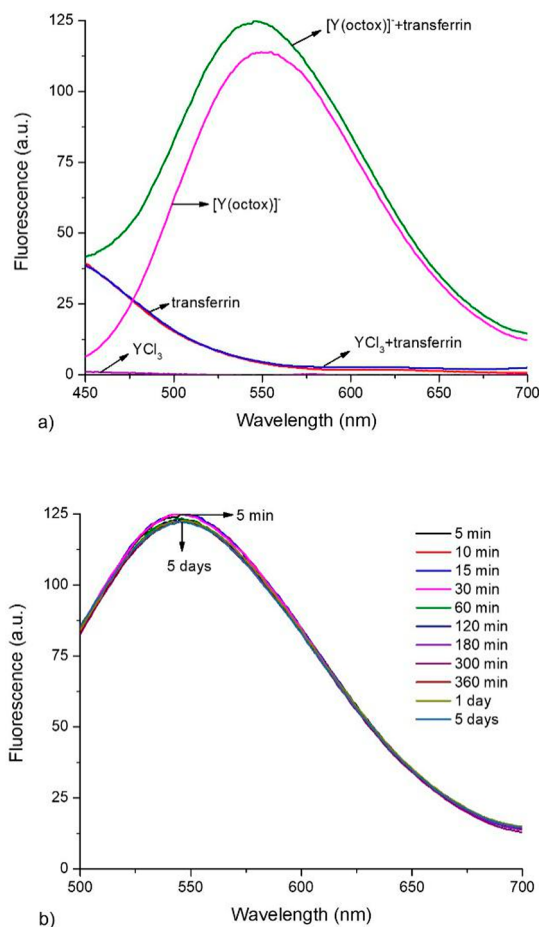**Figure 5.** Fluorescence spectra of H$_4$octox and its Y^{3+}, La^{3+}, Lu^{3+}, and In^{3+} complexes at pH 8 (λ_{exc} = 350 nm, [H$_4$octox] = [M(octox)]$^-$ = 2 × 10^{-4} M).

presents a really weak fluorescence, as do its complexes with In^{3+} at the same pH; however, when H$_4$octox is chelated to Y^{3+}, Lu^{3+}, and La^{3+} the fluorescence is notably enhanced, in particular for [Y(octox)]$^-$, a 60-fold increase. This property of H$_4$octox could be useful in the development of fluorescent chemosensors for tracing the intracellular distribution of cold metal bioconjugates without the need for further fluorescence tags, such as fluorescein, and, potentially, for the development of bimodal imaging contrast agents.

Stability Studies against Transferrin and Fe^{3+}. When evaluating the stability of radiometal complexes *in vivo*, kinetic inertness is of great importance, since native chelators (e.g., apo-transferrin, albumin) or metal ions (e.g., Fe^{3+}, Cu^{2+}, or Zn^{2+}) can compete for either the metal or the chelator in the radiopharmaceutical compound. *In vitro* competition experiments using endogenous chelators (transferrin) and endoge-

nous metal ions (Fe^{3+}) were performed taking advantage of the chelation-enhanced fluorescence (CHEF) emission of H$_4$octox and of the UV−vis spectra of its metal complexes.

Monitoring chelation-enhanced fluorescence (CHEF) of H$_4$octox, an *in vitro* stability study of [Y(octox)]$^-$ against transferrin was undertaken using non-radioactive metal ions. The fluorescence emission spectra of YCl$_3$ (5× 10^{-5} M), transferrin (1 mg/mL), and [Y(octox)]$^-$ (5 × 10^{-5} M) in PBS (pH 7.4) solutions were registered. As shown in Figure 6a,

Figure 6. (a) Fluorescence spectra of YCl$_3$ (5 × 10^{-5} M), transferrin (1 mg/mL), [Y(octox)]$^-$ (5 × 10^{-5} M), transferrin (1 mg/mL) + YCl$_3$ (5 × 10^{-5} M), and [Y(octox)]$^-$ (5 × 10^{-5} M) + transferrin (1 mg/mL) in PBS (pH 7.4) solution. (b) [Y(octox)]$^-$ complex stability study against transferrin.

while YCl$_3$ had no emission, transferrin showed very weak emission over the range 500−600 nm compared with [Y(octox)]$^-$. When YCl$_3$ was then added to a transferrin solution ([Y^{3+}] = 5 × 10^{-5} M), the emission spectrum showed little change and was still weak at 500−600 nm; therefore, when [Y(octox)]$^-$was incubated with transferrin, the intensity of fluorescence emission would decrease if the Y^{3+} was released or transchelated to transferrin. As presented in Figure 6b, the fluorescence emission of [Y(octox)]$^-$ (5 × 10−5 M) in

transferrin (1 mg/mL) was recorded for 5 days. The intensity of the peak emission decreased ~2% over 5 days, confirming excellent *in vitro* stability of $[Y(octox)]^-$ against transferrin.

Similarly, a Fe^{3+} transmetalation competition experiment was carried out by following the change in fluorescence of the $[Y(octox)]^-$ complex over the 72 h experiment since $[Fe(octox)]^-$ complex has no fluorescence emission. Also this experiment proved the great stability of the $[Y(octox)]^-$ complex against Fe^{3+} ions; otherwise the fluorescence would have quenched (Figure S9). The fluorescence emission of the $[Y(octox)]^-$ complex remained stable when it was incubated with 1 equiv of Fe^{3+}, and a ca. 2% decrease of the peak emission was observed after 72 h.

UV−vis spectrophotometry was used to evaluate the transmetalation of the $[In(octox)]^-$ complex in the presence of different amounts of Fe^{3+} ions. The $[In(octox)]^-$ complex was incubated with 1 and 5 equiv of Fe^{3+}, respectively, at pH = 7.4 (HEPES buffer) (Figures 7 and S10). As shown in Figure
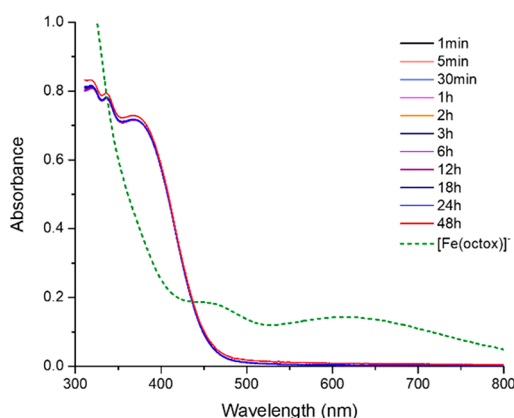
Figure 7. $[In(octox)]^-$ complex stability challenge against Fe^{3+}. UV−vis spectra of the $[In(octox)]^-$ complex (2×10^{-4} M) incubated with Fe^{3+}−citrate (2×10^{-4} M) at pH 7.4 (HEPES buffer).

7, the $[Fe(octox)]^-$ complex has a specific absorption band at around 625 nm, where $[In(octox)]^-$ does not absorb. In both experiments, the absorption spectra of the $[In(octox)]^-$ complex did not vary, and <3% increase at 625 nm was recorded after 48 h. These two experiments show the excellent stability of both $[In(octox)]^-$ and $[Y(octox)]^-$ against Fe^{3+}, which is important in order to avoid transmetalation reactions *in vivo*.

pH- and Temperature-Dependent $[^{111}In(octox)]^-$ Labeling. The high thermodynamic stability of $[In(octox)]^-$ in solution presaged good ^{111}In-labeling study results. The radiolabeling was conducted at two pH values and temperatures, and the results are summarized in Table 6. As shown

Table 6. Radiochemical Yields (RCY in %) of the Various Labeling Reactions Performed for the $^{111}In-H_4octox$ System

	ambient temperature		60 °C	
ligand concentration (M)	pH = 4	pH = 5.5	pH = 4	pH = 5.5
10^{-4}	96	97	98	100
10^{-5}	91	98	92	100
10^{-6}	5	97	92	99
10^{-7}	0	80	12	75
10^{-8}	−	8	−	53

there, pH 5.5 is better to ensure quantitative labeling at lower concentrations vs pH 4. This can be explained by the solution studies: the presence of protonated In(Hoctox) up to pH 5, where the ligand loses its last ionizable proton, from one of the phenol OH groups. Quantitative labeling was achieved at room temperature within 15 min with the concentration of the ligand being as low as $10^{-6}-10^{-7}$ M. This result supports the suitability for a kit-based application.

Serum Stability. Very often, serum stability studies are carried out using HPLC. In that case, the serum protein is denatured before radiochromatography, possibly destroying the chelation site of the proteins, and the transchelated metal ions could then be released and recombined quickly with the chelators, giving false positive results, especially for acyclic chelators like $H_4octapa$ and H_4octox with fast complexation kinetics. Therefore, a serum competition study using the PD-10 method was performed to further explore the *in vitro* stability of $[^{111}In(octox)]^-$; the results are presented and compared with data for previously reported chelators in Table 7. $[^{111}In(octox)]^-$ presents a high stability ($96.2 \pm 0.4\%$) after 1 h incubation in human serum. This exceeds the 1 h $^{111}In^{3+}$ competition values for $H_4octapa$, H_2dedpa, DOTA, DTPA, p-NH_2-Bn-CHX-A″-DTPA, and H_2bispa^2 chelators. As to the 24 h stability, it is still higher than for most. Although no data are available for many of the In chelators after 5 days, $[^{111}In(octox)]^-$ was 83.6% intact, with stability higher than that of DTPA, close to that of H_2bispa^2 and p-NH_2-Bn-CHX-A″-DTPA, and lower than that of p-NO_2-Bn-neunpa. It is noteworthy that serum stability data alone do not prove the superiority of one chelator over the others, as that depends also on the kinetics, thermodynamics, and experimental conditions used. For instance, in this serum competition study, the non-covalent binding of intact ^{111}In complex to the serum protein cannot be discerned and was counted as transchelation. The introduced error may be small and negligible when evaluating the previous hydrophilic chelators. Considering that $[^{111}In(octox)]^-$ is a hydrophobic anion and the tris(8-hydroxyquinolinato)indium complex was reported to have a significant non-covalent binding to human serum albumin (HSA),[43,44] the error from the non-covalent binding of $[^{111}In(octox)]^-$ to HSA might be significant, only underestimating the stability data. A phenomenon of transmetalation could also happen in serum, and in order to exclude that possibility the Fe^{3+} challenge experiments were performed as discussed above (Figure 7). Besides, some of the drawbacks of both P-10 column and HPLC serum stability methods discussed above add to the importance of our novel fluorescence-based stability experiments (both transferrin and Fe^{3+} challenges).

In Vivo Imaging of $[^{111}In(octox)]^-$. The 5 day $[^{111}In(octox)]^-$ *in vitro* stability suggested *in vivo* SPECT/CT imaging and biodistribution studies in mice. The addition of $^{111}InCl_3$ solution (3.22 mCi, 10 μL) to H_4octox in water (100 μL, 2 mM) produced $[^{111}In(octox)]^-$ at a radiochemical yield of 98% within 15 min at room temperature as confirmed by radio-HPLC. The radiocomplex $[^{111}In(octox)]^-$ eluted with nearly the same retention time ($t_R = 6.1$ min) as the non-radioactive In−octox complex (Figure 8) with only 5 s between the UV and gamma traces, a consequence of the sequential arrangement of the detectors. In contrast, the free ligand H_4octox alone eluted 1.4 min later ($t_R = 7.5$ min), indicating the more polar nature of the negatively charged complex compared to the ligand. Uncomplexed $^{111}InCl_3$ alone

Table 7. Mouse Serum Stability Challenges Performed at Ambient Temperature[a]

| complex	1 h stability	24 h stability	5 days stability
$[^{111}In(octox)]^-$	96.2 ± 0.4	91.4 ± 0.6	83.6 ± 1.4
$[^{111}In(dedpa)]^+$ [b]	96.1 ± 0.1	19.7 ± 1.5	NA
$[^{111}In(octapa)]^-$ [b]	93.8 ± 3.6	92.3 ± 0.04	NA
$[^{111}In(DOTA)]^-$ [b]	89.6 ± 2.1	89.4 ± 2.2	NA
$[^{111}In(DTPA)]^{2-}$ [b]	86.5 ± 2.2	88.3 ± 2.2	<60%[e]
$[^{111}In(p\text{-}NO_2\text{-}Bn\text{-}neunpa)]^-$ [c]	97.9 ± 0.3	97.8 ± 0.1	97.8 ± 0.7
$[^{111}In(p\text{-}NH_2\text{-}Bn\text{-}CHX\text{-}A''\text{-}DTPA)]^{2-}$ [c]	91.8 ± 1.8	89.9 ± 0.6	90.1 ± 0.9
$[^{111}In(bispa^2)]^+$ [d]	88.4 ± 1.2	87.4 ± 0.6	87.4 ± 1.5

[a]Stability shown as the percentage of intact ^{111}In complex. [b]From ref 14. [c]From ref 18. [d]From ref 17. [e]From ref 45.
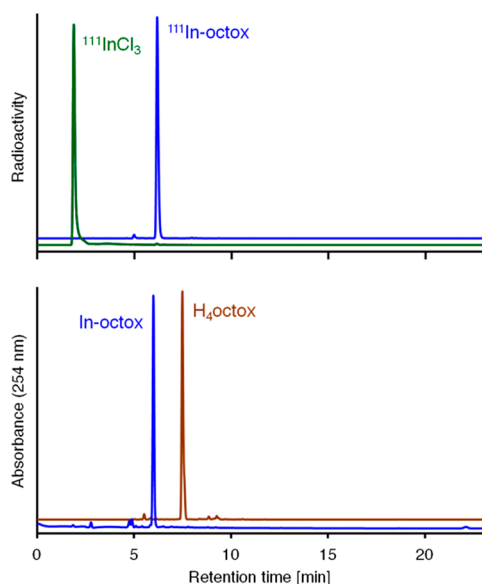
Figure 8. The $[^{111}In(octox)]^-$ radiocomplex (top, blue) elutes with nearly the same radio-HPLC retention time (t_R = 6.1 min) as the non-radioactive $[In(octox)]^-$ complex (bottom, blue). H_4octox (bottom, brown) elutes 1.4 min later, and $^{111}InCl_3$ (top, green) elutes with the mobile phase front.

eluted with the mobile phase front (t_R = 1.9 min). From the HPLC of each radiometal and non-radioactive complex, only one single sharp peak was observed (Figure 8), indicating that the two isomers found in solution by NMR have the same polarity and affect neither the purification nor the in vivo biodistribution.

Following intravenous administration, a portion of $[^{111}In-(octox)]^-$ is excreted through the urinary tract to the bladder, while the remaining is distributed to the liver, bile ducts, and gallbladder and excreted into the intestinal tract. Figure 9 illustrates longitudinal changes in the complex biodistribution over time. Dynamic SPECT/CT animated images of maximum intensity projections (MIPs) can be visualized in the Supporting Information (Movies S1 and S2). Assessment of the organ-specific time–activity curves for $[^{111}In(octox)]^-$ displayed differences in organ uptake and kinetics (Figure 10). Standardized uptake values (SUVs) of $[^{111}In(octox)]^-$ as
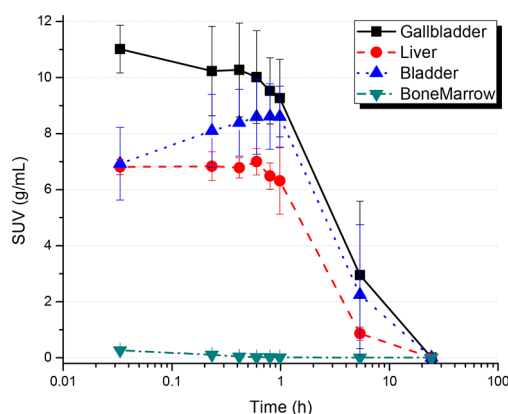
Figure 10. Representative SUV time–activity curves for $[^{111}In-(octox)]^-$ in mice (n = 3).

a function of time (n = 3) showed high liver and gallbladder activity within the first 5 min (Figure 10). About 26.0 ± 1.5% of the total $[^{111}In(octox)]^-$ complex was rapidly excreted within 60 min through the renal system, as shown by a very
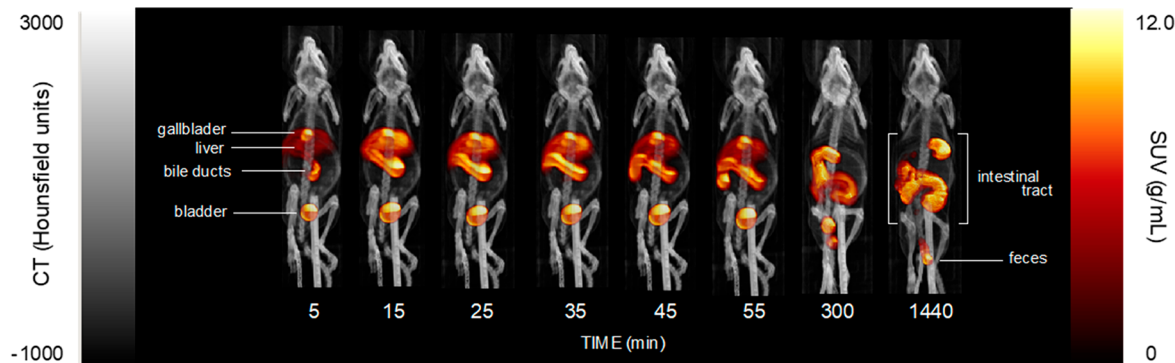
Figure 9. Top view maximum intensity projections (MIPs) on total body SPECT/CT scans at various time points after administration of $[^{111}In(octox)]^-$ complex. Additional dynamic SPECT and animated images of MIPs can be visualized in the SI (Movies S1 and S2).

quick and high activity increase in the bladder very early on (Figures 10 and 11, Movies S1 and S2 in the Supporting
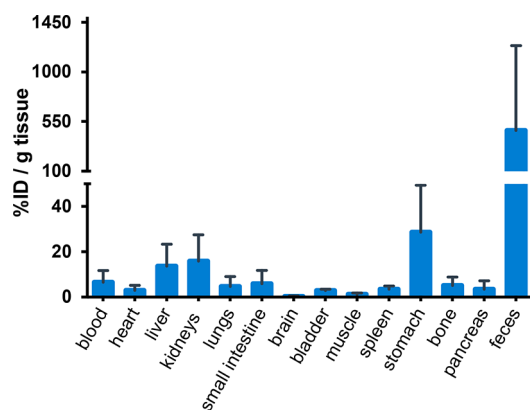
Figure 11. Biodistribution of $[^{111}In(octox)]^-$ after 24 h post-injection, $n = 3$. Percentage of injected dose per gram of organ weight.

Information). The kidneys, however, did not show measurable activity as the activity just seems to be passing through with no accumulation in kidney's cortex and medulla which could be an advantage over many previously reported chelators. In many peptide conjugates of DOTA, CHX-A″-DTPA, and particularly in DTPA kidney uptake is observed and it can decrease the imaging quality and minimize nephrotoxicity when using therapeutic isotopes such as $^{86/90}Y$ or ^{177}Lu.[6−8,46,47] Similarly, $32 \pm 2.5\%$ was eliminated through the liver and secreted into the bile (gallbladder) within the first hour post-injection. In the same time, the data show that $40 \pm 3.1\%$ of the initial $[^{111}In(octox)]^-$ was excreted into the intestinal tract from where it was excreted in the feces within 24 h post-administration (Figures 10 and 11).

This is consistent with the higher lipophilicity of H_4octox, unlike most previously reported multiarmed carboxylate- or picolinate-based chelators, which usually clear through the kidneys.[1,14] This could provide a complementary choice in tracer design and may have a (positive) impact on the pharmacokinetics or binding properties, especially for small molecules. For instance, studies with a PSMA inhibitor-based ^{68}Ga tracer revealed that using a more lipophilic chelator HBED-CC increased tumor uptake and reduced unspecific binding compared with the DOTA conjugate.[48,49] In a recent study, five different chelators were conjugated to the same RGD peptide and investigated to evaluate the effect of lipophilicity of the chelators on the pharmacokinetics of the bioconjugates.[50] This research also reported that those tracers using more lipophilic chelators show higher tumor uptake and tumor/organ ratios despite the increased liver uptake, versus those using polar hydrophilic chelators. In our own work with a ^{111}In-labeled trastuzumab bioconjugate applying a more lipophilic picolinate-based chelator H_4octapa showed a markedly higher tumor uptake than did ^{111}In−DOTA−trastuzumab, indicating that even for large biovectors such as an antibody the moderating effect of the chelating moiety on the pharmacokinetic properties may not be negligible.[51] Therefore, H_4octox provides an important, more hydrophobic complement for the currently used chelator library in manipulating the pharmacokinetics of the bioconjugates, considering that almost all of the currently used large trivalent

metal ion chelators are polar, resulting in fast clearance, possibly obviating tumor uptake.

Negligible activity accumulated in the bone marrow consistent with minimal dissociation and free $^{111}In^{3+}$ (Figures 9 and 10). In fact, the small amount of activity in the bone measured early is likely just the radioactivity of the radio-labeled complex in the bloodstream based on its fast disappearance. Moreover, no liver accumulation is shown after 5 h, indicating that it has a good metabolic stability in the liver with no metal release.

Analysis of the latest imaging time points (5 and 24 h) indicates that clearance of this compound occurs mainly through the gastrointestinal tract. This is again typical for lipophilic substances of this size, as for example shown with ^{99m}Tc-hepatobiliary iminodiacetic acid (HIDA).[52] The final passage through the intestine into the colon 24 h post-injection is well observed in the images (Figure 9).

Biodistribution of $[^{111}In(octox)]^-$. The radiolabeled complex is processed through enterohepatic circulation. This means that the complex enters the portal circulation, is taken up in the liver and potentially metabolized, and then returns to the gastrointestinal tract via biliary excretion. The complex leaves the body by excretion through the feces, as it is not reabsorbed in the intestine. This process depends heavily on the physicochemical properties (lipophilicity) of the compound and its alteration by the metabolism. The SPECT images clearly corroborate this process (Figure 9). This trend was further confirmed by the results obtained from the biodistribution study (Figure 11).

CONCLUSIONS

H_4octox incorporates the rigid oxine arm motif into an octadentate ligand for large metal ions and shows great potential for radiopharmaceuticals. The facile, inexpensive synthesis of this new chelator allows large-scale preparation and wide use. It shows both fast chelation kinetics with metal ions (Y^{3+}, In^{3+}, La^{3+}, Gd^{3+}, Lu^{3+}) as an acyclic chelator and high thermodynamic stability of the formed complexes resulting from the excellent geometry arrangement of the coordination atoms and rigidity of the formed chelate. The cavity of this preorganized chelator fits best $In^{3+} > Lu^{3+} > Y^{3+} > Gd^{3+} > La^{3+}$, following a trend of decreasing ionic radii, carrying a major advantage for the development of a versatile radiopharmaceutical agent. In the ^{111}In radiolabeling experiments, H_4octox achieves quantitative radiolabeling within 15 min at ambient conditions (pH 5.5 and room temperature) with ligand concentrations as low as $10^{-6}−10^{-7}$ M, and this is significant for developing kit-based radiopharmaceuticals, especially for thermally sensitive biovectors such as antibodies. The in vitro serum stability study together with in vivo SPECT/CT imaging and biodistribution data confirmed the good stability of radiometal-octox complexes with no persistent kidney uptake or liver accumulation in vivo. Moreover, the ligand is more lipophilic than most of the multiarmed carboxylate or picolinate chelators; therefore, it shows gastrointestinal clearance and provides a complementary choice for the design of metal-based pharmaceuticals and tuning of their pharmacokinetic properties. The chelation-enhanced fluorescence property was used to confirm an excellent in vitro stability of $[Y(octox)]^-$ against transferrin and Fe^{3+}, a unique advantage over the previously reported chelators in a "cold" metal-ion-based study. The intrinsic fluorescence of

[Y(octox)]⁻ and [Lu(octox)]⁻ could be potentially useful in intracellular fluorescence or a bimodal imaging tracer as well.

The high thermodynamic stability in solution, the turn-on fluorescence of H_4octox with Y^{3+} and Lu^{3+}, and the high [^{111}In(octox)]⁻ stability *in vivo* stimulate future studies with $^{86/90}$Y and ^{177}Lu. A bifunctional chelating analogue of this promising novel scaffold is currently under investigation, and further *in vivo* stability and biodistribution studies of the bifunctional analogue with ^{111}In, $^{86/90}$Y, and ^{177}Lu will be reported. Assessing liver histology, and/or evaluating the levels of different liver enzymes in blood, which are upregulated under the duress of toxicity, is interesting and should be examined in further experiments if this chelator is found to be useful as a diagnostic *in vivo* probe.

■ EXPERIMENTAL SECTION

Materials and Methods. All solvents and reagents were purchased from commercial sources (TCI America, Sigma-Aldrich, Fisher Scientific) and used as received unless otherwise indicated. The analytical thin-layer chromatography (TLC) plates used were aluminum-backed ultrapure silica gel 60 Å, 250 μm thickness. ^{1}H and ^{13}C NMR spectra were recorded at ambient temperature unless otherwise noted on Bruker AV300 and AV400 spectrometers; the ^{1}H NMR spectra were calibrated against residual protio-solvent peak, and the ^{13}C NMR spectra were referenced to the deuterated solvent. NOESY experiments were recorded on a Bruker AV400 spectrophotometer at 400.13 MHz. Low-resolution mass spectrometry was performed on a Waters ZG spectrometer with an ESCI (electrospray/chemical-ionization) source, and high-resolution electrospray ionization mass spectrometry (ESI-MS) was performed on a Micromass LCT time-of-flight (TOF) instrument. Microanalyses for C, H, and N were performed on a Carlo Erba elemental analyzer EA 1108. Purification and quality control of [^{111}In(octox)]⁻ for SPECT/CT imaging were performed on an Agilent HPLC system equipped with a model 1200 quaternary pump, a model 1200 UV absorbance detector, and a Bioscan (Washington, DC) NaI scintillation detector. The radio detector was connected to a Bioscan B-FC-1000 Flow-count system, and the output from the Bioscan Flow-count system was fed into an Agilent 35900E Interface which converted the analog signal to digital signal. The operation of the Agilent HPLC system was controlled using the Agilent ChemStation software. The HPLC columns used were a semipreparative column (Phenomenex C18, 5 μm, 250 × 10 mm) and an analytical column (Phenomenex C18, 5 μm, 250 × 4.6 mm). The HPLC solvents were (A) H_2O containing 0.1% TFA, and (B) CH_3CN containing 0.1% TFA. Radioactivity of [^{111}In(octox)]⁻ was measured using a Capintec (Ramsey, NJ) CRC-25R/W dose calibrator. SPECT imaging experiments were conducted using a Siemens (Erlangen, Germany) Inveon microPET/CT scanner. Human serum and Sephadex G-25 PD10 Desalting columns were purchased from Sigma-Aldrich and GE Healthcare, respectively. ^{111}In was obtained from Nordion Inc. (Vancouver, BC, Canada) as ^{111}InCl$_3$ in dilute HCl. pH- and temperature-dependent labeling studies of [^{111}In(octox)]⁻ were performed on a Waters Alliance e2696 separations module coupled to a Waters 2489 UV/vis detector (λ = 254 nm) and a LabLogic Scan-RAM radio detector operated at 950 V. The column was a reversed-phase C18 Waters Atlantis T3, 100 Å, 5 μm particle size (4.6 × 150 mm), supported by a C18 guard cartridge and was operated in an oven at 40 °C. The column was eluted with the following gradient: A = 0.1% trifluoroacetic acid (TFA) in water; B = acetonitrile; flow rate = 1 mL/min; 0−20 min 95% A; 20−23 min 100% B.

Synthesis and Characterization. *H_2hox (1).* H_2hox was synthesized following our reported procedure.[23] 8-Hydroxyquinoline-2-carboxaldehyde (11.6 mmol, 2 g) was dissolved in 50 mL of ethanol, and ethylenediamine (5.8 mmol, 387 μL) dissolved in 5 mL of ethanol was added dropwise; the reaction mixture was stirred at 60 °C for 4 h. A light-yellow precipitate formed and was collected and resuspended in 50 mL of ethanol. Five equivalents of NaBH$_4$ (29

mmol, 1.1 g) was added in portions, and the reaction mixture was stirred at room temperature overnight. HCl (20 mL, 6 M) was added, and the reaction mixture was stirred for 4 h to quench. The pH of the reaction mixture was adjusted to neutral using NaOH (2 M dropwise), and the white precipitate was filtered and dried as crude product (5.2 mmol, 1.97 g, yield = 91%). ^{1}H NMR (300 MHz, MeOD) δ 8.21 (d, J = 8.5 Hz, 1H), 7.50−7.38 (m, 2H), 7.36 (dd, J = 8.3, 1.6 Hz, 1H), 7.10 (dd, J = 7.3, 1.6 Hz, 1H), 4.20 (s, 2H), 3.03 (s, 2H). ^{13}C NMR (75 MHz, MeOD) δ 157.4, 154.1, 139.2, 138.1, 129.5, 128.4, 121.9, 119.0, 112.3, 54.7, 49.0, 48.8. HR-ESI-MS calcd for $C_{22}H_{23}N_4O_2$: 375.1821. Found: 375.1819 [M + H]$^+$. H_2hox·2HCl used for titration was synthesized by mixing a solution of H_2hox (2) in THF and 6 M HCl and drying in vacuo to afford a white powder. Anal. Calcd for H_2hox·2HCl·0.5 H_2O: C, 57.9; H, 5.52; N, 12.28. Found: C, 58.24; H, 5.30; N, 11.90.

Di-tert-Butyl 2,2′-(Ethane-1,2-diylbis(((8-hydroxyquinolin-2-yl)-methyl)azanediyl))diacetate (2). H_2hox (312 mg, 0.83 mmol) and NaHCO$_3$ (530 mg, 5 mmol, 6 equiv) were suspended in dry CH_3CN, and *tert*-butyl bromoacetate (1.84 mmol, 27 μL) was added dropwise. The mixture was stirred at 50 °C for 24 h and then filtered. The filtrate was collected and purified using column chromatography to obtain a light yellow powder (421 mg, 0.7 mmol, yield 84%) (CombiFlash Rf automated column system; 40 g of HP silica; A, hexane; B, EtOAc, 100% A to 80% B gradient). ^{1}H NMR (400 MHz, CD$_2$Cl$_2$) δ 8.05 (d, J = 8.5 Hz, 1H), 7.66 (d, J = 8.5 Hz, 1H), 7.43 (dd, J = 8.2, 7.6 Hz, 1H), 7.31 (dd, J = 8.3, 1.3 Hz, 1H), 7.16 (dd, J = 7.6, 1.3 Hz, 1H), 4.10 (s, 2H), 3.41 (s, 2H), 2.91 (s, 2H), 1.47 (s, 9H). ^{13}C NMR (101 MHz, CD$_2$Cl$_2$) δ 170.9, 158.9, 152.5, 137.7, 136.7, 128.0, 127.5, 122.5, 118.0, 110.2, 81.1, 61.0, 56.5, 52.5, 28.3. ^{13}C NMR (75 MHz, D$_2$O) δ 173.0, 151.7, 147.9, 143.6, 131.4, 129.7, 128.3, 120.8, 119.3, 114.7, 56.3, 55.9, 51.4.

H_4octox 4HCl·1.8H_2O (3). Compound **2** (103 mg, 0.171 mmol) was suspended in 6 M HCl, stirred at 60 °C overnight, and then vacuum dried to a yellow powder as the final product (111 mg, 0.166 mmol, yield = 97%). ^{1}H NMR (300 MHz, D$_2$O) δ 8.31 (d, J = 8.5 Hz, 1H), 7.49 (d, J = 8.5 Hz, 1H), 7.34 (t, J = 8.0 Hz, 1H), 7.24 (d, J = 8.2 Hz, 1H), 6.87 (d, J = 7.6 Hz, 1H), 4.46 (s, 2H), 3.85 (s, 2H), 3.51 (s, 2H). ^{13}C NMR (75 MHz, D$_2$O) δ 173.0, 151.7, 147.9, 143.6, 131.4, 129.7, 128.3, 120.8, 119.3, 114.7, 56.3, 55.9, 51.4. HR-ESI-MS calcd for $C_{26}H_{27}N_4O_6$: 491.1931. Found: 491.1930 [M + H]$^+$. Anal. Calcd for H_4octox·4HCl·1.8 H_2O: C, 46.69; H, 5.06; N, 8.38. Found: C, 46.63; H, 5.05; N, 8.56.

Na[In(octox)] (4). Compound **3** and In(ClO$_4$)$_3$ were mixed in H_2O, and NaOH (0.1 M) was used to adjust the pH to 8. The mixture was stirred at 50 °C overnight and then vacuum dried to obtain the product as a yellow powder. ^{13}C NMR (75 MHz, MeOD) δ 170.5, 153.0, 148.9, 144.7, 131.2, 130.0, 129.3, 122.0, 118.8, 115.1, 56.8, 55.1, 52.4. HR-ESI-MS calcd for $C_{26}H_{23}InN_4NaO_6$: 625.0554. Found: 625.0551 [M + H + Na]$^+$.

X-ray Crystallography. An irregular yellow crystal of $C_{104}H_{92}La_3N_{16}O_{26}$·6($H_2O$) having approximate dimensions of 0.08 × 0.10 × 0.25 mm was mounted on a cryo-loop. All measurements were made on a Bruker APEX DUO diffractometer with a TRIUMPH curved-crystal monochromator with Mo Kα radiation. The data were collected at a temperature of −183.0 ± 0.1 °C to a maximum 2θ value of 44.94° in a series of ϕ and ω scans in 0.5° oscillations using 15.0 s exposures. The crystal-to-detector distance was 40.16 mm. Of the 78 144 reflections collected, 17 280 were unique (R_{int} = 0.0734); equivalent reflections were merged. Data were collected and integrated using the Bruker SAINT[53] software package. The linear absorption coefficient, μ, for Mo Kα radiation is 10.16 cm^{-1}. Data were corrected for absorption effects using the multiscan technique (SADABS),[54] with minimum and maximum transmission coefficients of 0.8011 and 0.9219, respectively. The data were corrected for Lorentz and polarization effects. The structure was solved by direct methods.[55] The solvent regions could not be reasonably modeled; therefore, the PLATON/SQUEEZE[56] program was employed to generate "solvent-free" data. All non-hydrogen atoms were refined anisotropically, while all hydrogen atoms were refined isotropically. The standard deviation of an observation of unit weight was 1.00. The

weighting scheme was based on counting statistics. The maximum and minimum peaks on the final difference Fourier map corresponded to 2.71 and −1.03 e⁻/Å³, respectively. Neutral atom scattering factors were taken from Cromer and Waber.[57] Anomalous dispersion effects were included in Fcalc;[58] the values for $\Delta f'$ and $\Delta f''$ were those of Creagh and McAuley.[59] The values for the mass attenuation coefficients are those of Creagh and Hubbell.[60] All refinements were performed using SHELXL-2016[61] via the OLEX2[62] interface.

DFT Calculations. All calculations were performed using the Gaussian 09 package (Revision D.01). Full geometry optimizations of the $[In(octox)]^-$ and $[In(octapa)]^-$ anions were performed using the B3LYP hybrid functional[63,64] in aqueous solution using the polarizable continuum model (PCM).[65] Geometry optimizations were carried out using the 6-311+G(d,p) basis set on first- and second-row elements and the Los Alamos effect core potential (ECP) and valence basis set of double-ζ quality (LANL2DZ)[66–68] on the indium atom. The input coordinates of atoms were adapted from the crystal structure of the $[La_3(octox)_4]$ complex, and no constraints on symmetry were imposed during the geometry optimization. The resulting geometries showed no imaginary frequencies and thus were confirmed to be minima on the potential energy surfaces. The same functional, basis set, and ECP were employed to generate its ground state molecular electrostatic potential (MEP) mapping. The MEP was mapped onto the calculated electron density surface.

Solution Thermodynamics. Protonation constants and metal stability constants were obtained by combined UV−potentiometric titrations as described before[18,31,69] using a Metrohm Titrando 809 equipped with a Ross combined electrode, a Metrohm Dosino 800, and a Varian Cary 60 UV/vis spectrophotometer (200−450 nm spectral range) connected to a 0.2 cm path length optic dip probe immersed in the titration cell. The titration apparatus consisted of a 20 mL and 25 °C thermostatted glass cell and an inlet−outlet tube for nitrogen gas (purified through a 10% NaOH solution) to exclude any CO_2 prior to and during the course of the titration. The electrode was calibrated daily for hydrogen ion concentrations using a standard HCl as described before,[70] and the results were analyzed with the procedure of Gran.[71] Solutions were titrated with carbonate-free NaOH (0.16 M) that was standardized against freshly recrystallized potassium hydrogen phthalate. Protonation equilibria of the ligand were studied by joined potentiometric−spectrophotometric titrations of a solution containing H_4octox (9.55×10^{-4} M) at 25 °C, $l = 0.2$ cm, and 0.16 M NaCl ionic strength. Electromotive force values and spectra were recorded after each NaOH or HCl addition, and both apparatuses were synchronized in order to have constant delays between each titrant addition and sufficient time to equilibrium. The last two ligand protonation equilibria, outside the electrode threshold, were studied via in-batch UV−vis spectrophotometry on a set of solutions at the same ligand concentration ($[H_4octox] = 3.06 \times 10^{-5}$ M, $l = 1$ cm) containing different amounts of HCl. The equilibrium H^+ concentration in the UV in batch titration procedure at low-pH solutions (pH ≤ 2) was calculated from solution stoichiometry, not measured with a glass electrode. For the solutions of high acidity, the correct acidity scale H^0 was used.[72] In metal complexation studies with In(III) due to the strength of the metal complexes, two different methods were used: direct proton competition experiments and ligand−ligand competition with the known competitor EDTA. The first method used in batch UV−potentiometric measurements on a set of solutions containing a 1:1 metal to ligand molar ratio ($[H_4octox] = [In^{3+}] = 3.06 \times 10^{-5}$ M) and different amounts of HCl or NaOH in the spectral range 200−450 nm at 25 °C and 1 cm path length, and automated UV−potentiometric titrations—$[H_4octox] = [In^{3+}] = 8.13 \times 10^{-4}$ M, 25 °C, $I = 0.16$ M NaCl and 0.2 cm path length. The second method used ligand−ligand pH−potentiometric competition titrations with EDTA at $[H_4octox] = 9.86 \times 10^{-4}$ M, $[In^{3+}] = 3.12 \times 10^{-4}$ M and $[EDTA] = 2.91 \times 10^{-4}$ M, 25 °C, $I = 0.16$ M NaCl.

Complex formation equilibria with Y(III), La(III), or Gd(III) were studied by direct UV−potentiometric titrations of 1:1 metal to ligand molar ratio ($[H_4octox] = [M^{n+}] = 9.86 \times 10^{-4}$ M) at 25 °C, $I = 0.16$ M, and 0.2 cm path length. Metal solutions were prepared by adding the atomic absorption (AA) standard metal ion solutions to a H_4octox

solution of known concentration in a 1:1 metal to ligand molar ratio. The exact amount of acid present in the indium, lanthanum, gadolinium, yttrium, and lutetium standards was determined by Gran's method,[71] titrating equimolar solutions of the chosen metal ions and Na_2H_2−EDTA. All the potentiometric measurements were processed using the Hyperquad2013 software,[73] while the obtained spectrophotometric data were processed with the HypSpec2014 program.[29] The molar absorptivities of all protonated species of H_4octox were included in the metal stability calculations. Protonation constants of EDTA and its In^{3+} metal stability constants were taken from the literature,[74] while proton dissociation constants corresponding to hydrolysis of In(III), Y(III), La(III), Gd(III), and Lu(III) aqueous ions included in the calculations were taken from Baes and Mesmer.[75] The species formed in the studied systems are characterized by the general equilibrium: $pM + qH + rL = M_pH_qL_r$ (charges omitted). For convention, a complex containing a metal ion, M, proton, H, and ligand, L, has the general formula $M_pH_qL_r$. The stoichiometric indices p might also be 0 in the case of protonation equilibria, and negative values of q refer to proton removal from metal-ion-coordinated water, equivalent to hydroxide ion addition to the complex. The overall equilibrium constant for the formation of the complexes $M_pH_qL_r$ from its components is designated as log β. Stepwise equilibrium constants log K correspond to the difference in log units between the overall constants of sequentially protonated (or hydroxide) species. pM is defined as $(-\log[M^{n+}]_{free})$ and is always calculated at $[M^{n+}] = 1$ μM, $[L^{x-}] = 10$ μM, pH 7.4, and 25 °C.

pH- and Temperature-Dependent $[In(octox)]^-$ Labeling Procedure. All labeling reactions were over a 15 min period. The reaction mixture was kept at 1 mL with NaOAc buffer (10 mM, pH = 5.5) or NH_4OAc buffer (0.15 M, pH = 4) using approximately 80− 100 μCi of $^{111}In^{3+}$ and 100 μL of the appropriate H_4octox solution. The H_4octox solutions were prepared by dilution of a stock 1×10^{-3} M solution (2 mg of H_4octox in 3 mL of MQ H_2O). Two reaction conditions were varied in these experiments: pH (4 and 5.5) and temperature (room temperature and 60 °C). The reaction progress was monitored using HPLC and a 4 μm Synergy Hydro-RP Analytical column. A linear gradient of 0% → 100% B (A, 0.1% trifluoroacetic acid (TFA) in water; B, acetonitrile) over 20 min was used to separate the product. Radioactive product was detected with a Raytest GABI* HPLC Gamma Spectrometer.

Serum Stability. PD-10 desalting column method: A quantitatively labeled reaction (see radiolabeling methods) with ∼3 mCi of activity is divided into replicates, and each replicate is diluted to 1 mL. An equal volume (1 mL) of human serum was added to a quantitatively radiolabeled $[^{111}In(octox)]^-$ complex, and the mixture was incubated at 37 °C. At time points of 1 h, 1 day, and 5 days, a 400 μL aliquot (or 800 uL on day 5) was diluted to 2.5 mL and the activity was measured with the CRC55tR dose calibrator. The dilution was then loaded onto an equilibrated PD-10 desalting column, and the activity of the empty vial was measured to determine the "residual activity". Once the entire mixture has been adsorbed onto the column, the proteins (MW > 5000 Da) are eluted with 3.5 mL of PBS. The activity of the elution is then measured, and the stability of the complex in % is calculated as % stable = 1 − (activity of elution)/ ((activity of load) − (activity residual)).

Transmetalation Stability Against Fe^{3+}. $[In(octox)]^-$ (2×10^{-4} M) was incubated with 1 equiv of iron(III) citrate (2×10^{-4} M) or 5 equiv of iron(III) citrate (1×10^{-3} M) in HEPES (pH 7.4, 10 mM) solution; sodium citrate (citrate:Fe^{3+} = 3:1) was added to stabilize the Fe^{3+}. UV−vis spectra were measured using a Varian Cary 60 UV/vis spectrophotometer. For the fluorescence transmetalation study, $[Y(octox)]^-$ (2×10^{-4} M) was incubated with 1 equiv of iron(III) citrate (2×10^{-4} M) in HEPES (pH 7.4, 10 mM) solution; sodium citrate (citrate:Fe^{3+} = 3:1) was added to stabilize the Fe^{3+}. Fluorescence emission spectra were measured at excitation wavelength $\lambda_{exc} = 350$ nm using an Agilent Cary Eclipse fluorescence spectrophotometer.

^{111}In Radiolabeling of H_4octox for *In Vivo* Studies. $^{111}InCl_3$ (3.22 mCi, 10 μL, in dilute HCl, Nordion Inc., Canada) was added to a fresh aqueous solution of H_4octox (100 μL, 2 mM), the pH was

raised to pH ≈ 7 by addition of Na_2CO_3 (5 μL, 0.1 M), and the mixture was agitated (350 rpm) at room temperature for 15 min. An aliquot was analyzed by radio-HPLC, confirming 98% radiolabeling. Radio-HPLC $[^{111}In(octox)]^-$: t_R = 6.1 min. Doses for animal injections were prepared by diluting 78 μL of the above solution with PBS (530 μL, pH 7.4).

In Vivo **SPECT/CT Imaging.** This was performed in accordance with the Canadian Council on Animal Care (CCAC) and protocol approved by the Animal Care Committee (ACC) of the University of British Columbia (A16-0150). Three healthy C57Bl/6 female mice (∼16 g) were anaesthetized using isoflurane on a precision vaporizer (5% in oxygen for induction, between 1.5% and 2.5% in oxygen for maintenance) and received a subcutaneous injection of lactated Ringer's solution (0.5 mL) for hydration prior to each imaging scan. After the induction of anesthesia, an injection containing 120 μL of $[^{111}In(octox)]^-$ in PBS was administered via a tail vein. Average injected activity was 310 μCi. Immediately after injection, dynamic whole-body images were acquired during 60 min using a multimodal SPECT/CT scanner (VECTor/CT, MILabs, The Netherlands) equipped with an XUHS-2 mm mouse pinhole collimator. Six frames of 10 min were acquired for the first hour scan. Thereafter, acquisitions were done at 5 and 24 h post-radiotracer injection using a single frame of 40 and 60 min, respectively. Throughout the entire scanning procedure the mouse was kept under isoflurane anesthesia, and constant body temperature was maintained using a heating pad. Following each SPECT acquisition, a whole-body CT scan was acquired to obtain anatomical information, and both images were registered. The ^{111}In photopeak window was centered at 171 keV with a 20% energy window width. For quantitative analysis, SPECT image reconstructions were carried out with a pixel-ordered subset expectation maximization (POSEM) algorithm that included resolution recovery and compensation for distance-dependent pinhole sensitivity. For the SPECT images, we used 16 subsets, 10 iterations, and an isotropic 0.4 mm voxel grid. The images were decay corrected, and after CT registration, attenuation correction was applied. For visual representation, the reconstructed volumes of SPECT scans were post-filtered with a 3D Gaussian filter. CT scans were acquired with a tube setting of 55 kV and 615 μA. In total 2 frames of 180 projections over 360° were acquired in step and shoot rotation mode. The acquired projection data was reconstructed using SkyScan NRecon software to generate a 3D CT image on 0.169 mm^3 voxel size. Volumes of interest (VOIs) were manually defined using AMIDE (v.1.0.5) to determine the time−activity pattern per target organ. Thus, the delineated regions were liver, bladder, bone, and gallbladder. The average organ activity per volume was obtained from the SPECT images, and the standardized uptake value (SUV) was extracted from each organ. In order to relate the scanner units (counts/voxel) to radioactivity concentration, a calibration factor was determined scanning a source with a known concentration of ^{111}In. Mice were sacrificed for ex vivo biodistribution, and the radioactivity in diverse organs was determined by γ counting.

Biodistribution of $[^{111}In(octox)]^-$. A full biodistribution was conducted (blood, heart, liver, kidneys, lungs, small intestine, brain, bladder, muscle, spleen, stomach, bone, tumor, pancreas, and feces) following the last scan at 24 h post-injection (Figure 9). Organs were cleaned from blood and weighed, and the activity was determined using a γ-counter (Packard Cobra II autogamma counter, PerkinElmer, Waltham, MA, USA). The calibration factor for 37 kBq of ^{111}In was 78 395 cpm (instrument specific). Total organ weights were used for the calculations of injected dose per gram of tissue (% ID/g organ) except for blood, liver, muscle, bone, and pancreas, where average literature values were used.

Fluorescence Spectra. Solutions of H_4octox and its respective metal complexes with Y^{3+}, Lu^{3+}, La^{3+}, and In^{3+} ($[H_4octox]$ = 2×10^{-4} M and 1:1 metal to ligand molar ratios) were prepared in Milli-Q water, and the pH was adjusted to 8 by adding NaOH (0.1 M). Fluorescence emission spectra were measured at excitation wavelength λ_{exc} = 350 nm using an Agilent Cary Eclipse fluorescence spectrophotometer.

■ ASSOCIATED CONTENT

ⓢ Supporting Information

The Supporting Information is available free of charge on the ACS Publications website at DOI: 10.1021/jacs.8b09964.

Protonation constants of H_4octox, representative spectra of the in batch UV spectrophotometric titration of 3.06×10^{-5} M H_2O solution of H_4octox, representative spectra of the simultaneous UV−potentiometric titration of 9.55×10^{-4} M solution of H_4octox, speciation plots of H_4octox calculated using protonation constants in Table 3, representative spectra of the UV−potentiometric titration of the Y^{3+}−H_4octox system, representative spectra of the UV−potentiometric titration of the La^{3+}−H_4octox system, representative spectra of the UV−potentiometric titration of the Gd^{3+}−H_4octox system, representative spectra of the UV−potentiometric titration of the Lu^{3+}−H_4octox system, representative spectra of the in batch UV spectrophotometric titration of the In^{3+}−H_4octox system, $[Y(octox)]^-$ complex stability challenge against 5 equiv of Fe^{3+}, $[In(octox)]^-$ complex stability challenge against 5 equiv of Fe^{3+}, ^1H NMR spectrum of compound **2** in CD_2Cl_2, ^{13}C NMR spectrum of compound **2** in CD_2Cl_2, ^1H NMR spectrum of H_4octox (**3**) in D_2O, ^{13}C NMR spectrum of H_4octox (**3**) in D_2O, ^1H NMR spectrum of $Na[In(octox)]$ in D_2O, 2D NOESY spectrum of $Na[In(octox)]$ in D_2O, ORTEP diagram of the $[La_3(octox)_4]^{7-}$·6H2O, crystallographic data for the La-octox structure, DFT-optimized structures and MEP mappings of isomers of $[In(octox)]^-$ and $[In(octapa)]^-$ (PDF)

Dynamic SPECT/CT animated images of maximum intensity projections (top view) (MPG)

Dynamic SPECT/CT animated images of maximum intensity projections (3D view) (MPG)

(CIF)

■ AUTHOR INFORMATION

Corresponding Author

*orvig@chem.ubc.ca

ORCID ⊙

María de Guadalupe Jaraquemada-Peláez: 0000-0002-6204-707X

Cristina Rodríguez-Rodríguez: 0000-0002-3313-4422

Yang Cao: 0000-0001-8636-7919

Christian Buchwalder: 0000-0001-5577-8870

Chris Orvig: 0000-0002-2830-5493

Notes

The authors declare no competing financial interest.

■ ACKNOWLEDGMENTS

■ REFERENCES

(1) Price, E. W.; Orvig, C. Matching chelators to radiometals for radiopharmaceuticals. *Chem. Soc. Rev.* **2014**, *43*, 260.

(2) Holland, J. P.; Williamson, M. J.; Lewis, J. S. Unconventional nuclides for radiopharmaceuticals. *Mol. Imaging* **2010**, *9*, 1.

(3) Lubberink, M.; Tolmachev, V.; Widstrom, C.; Bruskin, A.; Lundqvist, H.; Westlin, J. E. ^{110m}In-DTPA-D-Phe1-octreotide for imaging of neuroendocrine tumors with PET. *J. Nucl. Med.* **2002**, *43*, 1391.

(4) Pauwels, S.; Barone, R.; Walrand, S.; Borson-Chazot, F.; Valkema, R.; Kvols, L. K.; Krenning, E. P.; Jamar, F. Practical dosimetry of peptide receptor radionuclide therapy with ^{90}Y-labeled somatostatin analogs. *J. Nucl. Med.* **2005**, *46*, 92S.

(5) Banerjee, S.; Pillai, M. R.; Knapp, F. F. Lutetium-177 therapeutic radiopharmaceuticals: linking chemistry, radiochemistry, and practical applications. *Chem. Rev.* **2015**, *115*, 2934.

(6) Carrasquillo, J. A.; White, J. D.; Paik, C. H.; Raubitschek, A.; Le, N.; Rotman, M.; Brechbiel, M. W.; Gansow, O. A.; Top, L. E.; Perentesis, P.; Reynolds, J. C.; Nelson, D. L.; Waldmann, T. A. Similarities and differences in ^{111}In- and ^{90}Y-labeled 1B4M-DTPA antiTac monoclonal antibody distribution. *J. Nucl. Med.* **1999**, *40*, 268.

(7) Forster, G. J.; Engelbach, M. J.; Brockmann, J. J.; Reber, H. J.; Buchholz, H. G.; Macke, H. R.; Rosch, F. R.; Herzog, H. R.; Bartenstein, P. R. Preliminary data on biodistribution and dosimetry for therapy planning of somatostatin receptor positive tumours: comparison of ^{86}Y-DOTATOC and ^{111}In-DTPA-octreotide. *Eur. J. Nucl. Med. Mol. Imaging* **2001**, *28*, 1743.

(8) Camera, L.; Kinuya, S.; Garmestani, K.; Wu, C.; Brechbiel, M. W.; Pai, L. H.; McMurry, T. J.; Gansow, O. A.; Pastan, I.; Paik, C. H.; Carrasqufflo, J. A. Evaluation of the serum stability and in vivo biodistribution of CHX-DTPA and other ligands for yttrium labeling of monoclonal antibodies. *J. Nucl. Med.* **1994**, *35*, 882.

(9) Hnatowich, D. J.; Virzi, F.; Doherty, P. W. DTPA-coupled antibodies labeled with yttrium-90. *J. Nucl. Med.* **1985**, *26*, 503.

(10) Griffiths, G. L.; Govindan, S. V.; Sharkey, R. M.; Fisher, D. R.; Goldenberg, D. M. ^{90}Y-DOTA-hLL2: an agent for radioimmunotherapy of non-Hodgkin's lymphoma. *J. Nucl. Med.* **2003**, *44*, 77.

(11) Gad, S. C. *Handbook of pharmaceutical biotechnology*; Wiley-Interscience: Hoboken, NJ, 2007.

(12) EMA's final opinion confirms restrictions on use of linear gadolinium agents in body scans. European Medicines Agency, 2017; http://www.ema.europa.eu/ema/index.jsp?curl=pages/medicines/human/referrals/Gadolinium-containing_contrast_agents/human_referral_prac_000056.jsp&mid=WC0b01ac05805c516f (accessed Aug 28, 2018).

(13) Tircso, G.; Benyo, E. T.; Suh, E. H.; Jurek, P.; Kiefer, G. E.; Sherry, A. D.; Kovacs, Z. (S)-5-(p-nitrobenzyl)-PCTA, a promising bifunctional ligand with advantageous metal ion complexation kinetics. *Bioconjugate Chem.* **2009**, *20*, 565.

(14) Price, E. W.; Cawthray, J. F.; Bailey, G. A.; Ferreira, C. L.; Boros, E.; Adam, M. J.; Orvig, C. H$_4$octapa: an acyclic chelator for ^{111}In radiopharmaceuticals. *J. Am. Chem. Soc.* **2012**, *134*, 8670.

(15) Baranyai, Z.; Uggeri, F.; Giovenzana, G. B.; Benyei, A.; Brucher, E.; Aime, S. Equilibrium and kinetic properties of the lanthanoids(III) and various divalent metal complexes of the heptadentate ligand AAZTA. *Chem. - Eur. J.* **2009**, *15*, 1696.

(16) Chong, H. S.; Garmestani, K.; Ma, D.; Milenic, D. E.; Overstreet, T.; Brechbiel, M. W. Synthesis and biological evaluation of novel macrocyclic ligands with pendent donor groups as potential yttrium chelators for radioimmunotherapy with improved complex formation kinetics. *J. Med. Chem.* **2002**, *45*, 3458.

(17) Comba, P.; Jermilova, U.; Orvig, C.; Patrick, B. O.; Ramogida, C. F.; Ruck, K.; Schneider, C.; Starke, M. Octadentate Picolinic Acid-Based Bispidine Ligand for Radiometal Ions. *Chem. - Eur. J.* **2017**, *23*, 15945.

(18) Spreckelmeyer, S.; Ramogida, C. F.; Rousseau, J.; Arane, K.; Bratanovic, I.; Colpo, N.; Jermilova, U.; Dias, G. M.; Dude, I.; Jaraquemada-Pelaez, M. G.; Benard, F.; Schaffer, P.; Orvig, C. p-NO2-Bn-H4neunpa and H4neunpa-Trastuzumab: Bifunctional Chelator for Radiometalpharmaceuticals and ^{111}In Immuno-Single Photon Emission Computed Tomography Imaging. *Bioconjugate Chem.* **2017**, *28*, 2145.

(19) Tircso, G.; Kovacs, Z.; Sherry, A. D. Equilibrium and formation/dissociation kinetics of some Ln(III)PCTA complexes. *Inorg. Chem.* **2006**, *45*, 9269.

(20) Brechbiel, M. W.; Gansow, O. A.; Pippin, C. G.; Rogers, R. D.; Planalp, R. P. Preparation of the Novel Chelating Agent N-(2-Aminoethyl)-trans-1,2-diaminocyclohexane-N,N′,N″-pentaacetic Acid (H$_5$CyDTPA), a Preorganized Analogue of Diethylenetriaminepentaacetic Acid (H$_5$DTPA), and the Structures of Bi^{III}(CyDTPA)$^{2-}$ and Bi^{III}(H$_2$DTPA) Complexes. *Inorg. Chem.* **1996**, *35*, 6343.

(21) Stimmel, J. B.; Stockstill, M. E.; Kull, F. C. Yttrium-90 Chelation Properties of Tetraazatetraacetic Acid Macrocycles, Diethylenetriaminepentaacetic Acid Analogs, and a Novel Terpyridine Acyclic Chelator. *Bioconjugate Chem.* **1995**, *6*, 219.

(22) Van Nostrand, D.; Abreu, S. H.; Callaghan, J. J.; Atkins, F. B.; Stoops, H. C.; Savory, C. G. In-111-labeled white blood cell uptake in noninfected closed fracture in humans: prospective study. *Radiology* **1988**, *167*, 495.

(23) Wang, X.; Jaraquemada-Pelaez, M. G.; Cao, Y.; Pan, J.; Lin, K. S.; Patrick, B. O.; Orvig, C. H$_2$hox: Dual-Channel Oxine-Derived Acyclic Chelating Ligand for ^{68}Ga Radiopharmaceuticals. *Inorg. Chem.* **2018**, DOI: 10.1021/acs.inorgchem.8b01208.

(24) Spek, A. L. PLATON SQUEEZE: a tool for the calculation of the disordered solvent contribution to the calculated structure factors. *Acta Crystallogr., Sect. C: Struct. Chem.* **2015**, *71*, 9.

(25) Harris, W. R.; Carrano, C. J.; Raymond, K. N. Spectrophotometric Determination of the Proton-Dependent Stability Constant of Ferric Enterobactin. *J. Am. Chem. Soc.* **1979**, *101*, 2213.

(26) Liu, Z. D.; Khodr, H. H.; Liu, D. Y.; Lu, S. L.; Hider, R. C. Synthesis, Physicochemical Characterization, and Biological Evaluation of 2-(1′-Hydroxyalkyl)-3-hydroxypyridin-4-ones: Novel Iron Chelators with Enhanced pFe^{3+} Values. *J. Med. Chem.* **1999**, *42*, 4814.

(27) Crisponi, G.; Nurchi, V. M. *Chelation Therapy in the Treatment of Metal Intoxication*; Academic Press: Boston, 2016; p 35.

(28) Tabata, M. *Conditional Constants, The IUPAC Stability Constants Database*; Academic Software, 1993.

(29) Gans, P.; Sabatini, A.; Vacca, A. Determination of equilibrium constants from spectrophometric data obtained from solutions of known pH: The program pHab. *Ann. Chim.* **1999**, *89*, 45.

(30) Shannon, R. D. Revised Effective Ionic-Radii and Systematic Studies of Interatomic Distances in Halides and Chalcogenides. *Acta Crystallogr., Sect. A: Cryst. Phys., Diffr., Theor. Gen. Crystallogr.* **1976**, *32*, 751.

(31) Jaraquemada-Pelaez, M. G.; Wang, X.; Clough, T. J.; Cao, Y.; Choudhary, N.; Emler, K.; Patrick, B. O.; Orvig, C. H$_4$octapa: synthesis, solution equilibria and complexes with useful radiopharmaceutical metal ions. *Dalton Trans.* **2017**, *46*, 14647.

(32) Bardez, E.; Devol, I.; Larrey, B.; Valeur, B. Excited-state processes in 8-hydroxyquinoline: Photoinduced tautomerization and solvation effects. *J. Phys. Chem. B* **1997**, *101*, 7786.

(33) Goldman, M.; Wehry, E. L. Environmental Effects Upon Fluorescence of 5-Hydroxyquinoline and 8-Hydroxyquinoline. *Anal. Chem.* **1970**, *42*, 1178.

(34) Prodi, L.; Bargossi, C.; Montalti, M.; Zaccheroni, N.; Su, N.; Bradshaw, J. S.; Izatt, R. M.; Savage, P. B. An effective fluorescent chemosensor for mercury ions. *J. Am. Chem. Soc.* **2000**, *122*, 6769.

(35) Prodi, L.; Montalti, M.; Zaccheroni, N.; Bradshaw, J. S.; Izatt, R. M.; Savage, P. B. Characterization of 5-chloro-8-methoxyquinoline appended diaza-18-crown-6 as a chemosensor for cadmium. *Tetrahedron Lett.* **2001**, *42*, 2941.

(36) Segura, M.; Bricoli, B.; Casnati, A.; Munoz, E. M.; Sansone, F.; Ungaro, R.; Vicent, C. A prototype calix[4]arene-based receptor for carbohydrate recognition containing peptide and phosphate binding groups. *J. Org. Chem.* **2003**, *68*, 6296.

(37) Bronson, R. T.; Montalti, M.; Prodi, L.; Zaccheroni, N.; Lamb, R. D.; Dalley, N. K.; Izatt, R. M.; Bradshaw, J. S.; Savage, P. B. Origins

of 'on-off' fluorescent behavior of 8-hydroxyquinoline containing chemosensors. *Tetrahedron* **2004**, *60*, 11139.

(38) Zhang, H.; Han, L. F.; Zachariasse, K. A.; Jiang, Y. B. 8-Hydroxyquinoline benzoates as highly sensitive fluorescent chemosensors for transition metal ions. *Org. Lett.* **2005**, *7*, 4217.

(39) Rahier, R.; Noiriel, A.; Abousalham, A. Development of a Direct and Continuous Phospholipase D Assay Based on the Chelation-Enhanced Fluorescence Property of 8-Hydroxyquinoline. *Anal. Chem.* **2016**, *88*, 666.

(40) Jiang, X. H.; Wang, B. D.; Yang, Z. Y.; Liu, Y. C.; Li, T. R.; Liu, Z. C. 8-Hydroxyquinoline-5-carbaldehyde Schiff-base as a highly selective and sensitive Al^{3+} sensor in weak acid aqueous medium. *Inorg. Chem. Commun.* **2011**, *14*, 1224.

(41) Moon, S. Y.; Cha, N. R.; Kim, Y. H.; Chang, S. K. New Hg^{2+}-selective chromo- and fluoroionophore based upon 8-hydroxyquinoline. *J. Org. Chem.* **2004**, *69*, 181.

(42) Farruggia, G.; Iotti, S.; Prodi, L.; Montalti, M.; Zaccheroni, N.; Savage, P. B.; Trapani, V.; Sale, P.; Wolf, F. I. 8-Hydroxyquinoline derivatives as fluorescent sensors for magnesium in living cells. *J. Am. Chem. Soc.* **2006**, *128*, 344.

(43) Enyedy, E. A.; Domotor, O.; Bali, K.; Hetenyi, A.; Tuccinardi, T.; Keppler, B. K. Interaction of the anticancer gallium(III) complexes of 8-hydroxyquinoline and maltol with human serum proteins. *JBIC, J. Biol. Inorg. Chem.* **2015**, *20*, 77.

(44) Abou-Zied, O. K.; Al-Lawatia, N.; Elstner, M.; Steinbrecher, T. B. Binding of hydroxyquinoline probes to human serum albumin: combining molecular modeling and Forster's resonance energy transfer spectroscopy to understand flexible ligand binding. *J. Phys. Chem. B* **2013**, *117*, 1062.

(45) Paik, C. H.; Herman, D. E.; Eckelman, W. C.; Reba, R. C. Synthesis, plasma clearance, and in vitro stability of protein containing a conjugated indium-111 chelate. *J. Radioanal. Chem.* **1980**, *57*, 553.

(46) Wadas, T. J.; Wong, E. H.; Weisman, G. R.; Anderson, C. J. Coordinating radiometals of copper, gallium, indium, yttrium, and zirconium for PET and SPECT imaging of disease. *Chem. Rev.* **2010**, *110*, 2858.

(47) Wei, L.; Zhang, X.; Gallazzi, F.; Miao, Y.; Jin, X.; Brechbiel, M. W.; Xu, H.; Clifford, T.; Welch, M. J.; Lewis, J. S.; Quinn, T. P. Melanoma imaging using [111]In-, [86]Y- and ^{68}Ga-labeled CHX-A″-Re(Arg11)CCMSH. *Nucl. Med. Biol.* **2009**, *36*, 345.

(48) Eder, M.; Schafer, M.; Bauder-Wust, U.; Hull, W. E.; Wangler, C.; Mier, W.; Haberkorn, U.; Eisenhut, M. ^{68}Ga-complex lipophilicity and the targeting property of a urea-based PSMA inhibitor for PET imaging. *Bioconjugate Chem.* **2012**, *23*, 688.

(49) Eder, M.; Neels, O.; Muller, M.; Bauder-Wust, U.; Remde, Y.; Schafer, M.; Hennrich, U.; Eisenhut, M.; Afshar-Oromieh, A.; Haberkorn, U.; Kopka, K. Novel Preclinical and Radiopharmaceutical Aspects of [68Ga]Ga-PSMA-HBED-CC: A New PET Tracer for Imaging of Prostate Cancer. *Pharmaceuticals* **2014**, *7*, 779.

(50) Sarkar, S.; Bhatt, N.; Ha, Y. S.; Huynh, P. T.; Soni, N.; Lee, W.; Lee, Y. J.; Kim, J. Y.; Pandya, D. N.; An, G. I.; Lee, K. C.; Chang, Y.; Yoo, J. High in Vivo Stability of Cu-64-Labeled Cross-Bridged Chelators Is a Crucial Factor in Improved Tumor Imaging of RGD Peptide Conjugates. *J. Med. Chem.* **2018**, *61*, 385.

(51) Price, E. W.; Zeglis, B. M.; Cawthray, J. F.; Ramogida, C. F.; Ramos, N.; Lewis, J. S.; Adam, M. J.; Orvig, C. H_4octapa-trastuzumab: versatile acyclic chelate system for 111In and 177Lu imaging and therapy. *J. Am. Chem. Soc.* **2013**, *135*, 12707.

(52) Lambie, H.; Cook, A. M.; Scarsbrook, A. F.; Lodge, J. P.; Robinson, P. J.; Chowdhury, F. U. Tc99m-hepatobiliary iminodiacetic acid (HIDA) scintigraphy in clinical practice. *Clin. Radiol.* **2011**, *66*, 1094.

(53) *SAINT*, Version 8.34A; Bruker AXS Inc.: Madison, WI, 1997–2013.

(54) Krause, L.; Herbst-Irmer, R.; Sheldrick, G. M.; Stalke, D. Comparison of silver and molybdenum microfocus X-ray sources for single-crystal structure determination. *J. Appl. Crystallogr.* **2015**, *48*, 3.

(55) Sheldrick, G. M. SHELXT - integrated space-group and crystal-structure determination. *Acta Crystallogr., Sect. A: Found. Adv.* **2015**, *71*, 3.

(56) Spek, A. L. PLATON SQUEEZE: a tool for the calculation of the disordered solvent contribution to the calculated structure factors. *Acta Crystallogr., Sect. C: Struct. Chem.* **2015**, *71*, 9.

(57) Cromer, D. T. W. J. T. *International Tables for X-ray Crystallography*; Kluwer Academic Publishers: Boston, 1974; Vol. *IV*.

(58) Ibers, J. A.; Hamilton, W. C. Dispersion Corrections + Crystal Structure Refinements. *Acta Crystallogr.* **1964**, *17*, 781.

(59) Creagh, D. C. M. W. J. *International Tables for Crystallography*; Kluwer Academic Publishers: Boston, 1992; Vol. *C*, Table 4.2.6.8, pp 219–222.

(60) Creagh, D. C. H. J. H. *International Tables for Crystallography*; Kluwer Academic Publishers: Boston, 1992; Vol. *C*, Table 4.2.4.3, pp 200–206.

(61) Sheldrick, G. M. Crystal structure refinement with SHELXL. *Acta Crystallogr., Sect. C: Struct. Chem.* **2015**, *71*, 3.

(62) Dolomanov, O. V.; Bourhis, L. J.; Gildea, R. J.; Howard, J. A. K.; Puschmann, H. OLEX2: a complete structure solution, refinement and analysis program. *J. Appl. Crystallogr.* **2009**, *42*, 339.

(63) Stephens, P. J.; Devlin, F. J.; Chabalowski, C. F.; Frisch, M. J. Ab Initio Calculation of Vibrational Absorption and Circular Dichroism Spectra Using Density Functional Force Fields. *J. Phys. Chem.* **1994**, *98*, 11623.

(64) Becke, A. D. Density-functional thermochemistry. III. The role of exact exchange. *J. Chem. Phys.* **1993**, *98*, 5648.

(65) Caricato, M. Exploring Potential Energy Surfaces of Electronic Excited States in Solution with the EOM-CCSD-PCM Method. *J. Chem. Theory Comput.* **2012**, *8*, 5081.

(66) Hay, P. J.; Wadt, W. R. Ab initio effective core potentials for molecular calculations. Potentials for K to Au including the outermost core orbitals. *J. Chem. Phys.* **1985**, *82*, 299.

(67) Wadt, W. R.; Hay, P. J. Ab initio effective core potentials for molecular calculations. Potentials for main group elements Na to Bi. *J. Chem. Phys.* **1985**, *82*, 284.

(68) Hay, P. J.; Wadt, W. R. Ab initio effective core potentials for molecular calculations. Potentials for the transition metal atoms Sc to Hg. *J. Chem. Phys.* **1985**, *82*, 270.

(69) Nurchi, V. M. M.; Jaraquemada-Pelaez, M. d. G.; Lachowicz, J. I. I.; Zoroddu, M. A.; Peana, M. F.; Dominguez-Martin, A.; Choquesillo-Lazarte, D.; Remelli, M.; Szewczuk, Z.; Crisponi, G. Looking at new ligands for chelation therapy. *New J. Chem.* **2018**, *42*, 8021.

(70) Weekes, D. M.; Ramogida, C. F.; Jaraquemada-Pelaez, M. G.; Patrick, B. O.; Apte, C.; Kostelnik, T. I.; Cawthray, J. F.; Murphy, L.; Orvig, C. Dipicolinate Complexes of Gallium(III) and Lanthanum(III). *Inorg. Chem.* **2016**, *55*, 12544.

(71) Gran, G. Determination of the equivalence point in potentiometric titrations. Part II. *Analyst* **1952**, *77*, 661.

(72) Paul, M.; Long, F. H0 and related indicator acidity function. *Chem. Rev.* **1957**, *57*, 1.

(73) Gans, P.; Sabatini, A.; Vacca, A. Investigation of equilibria in solution. Determination of equilibrium constants with the HYPER-QUAD suite of programs. *Talanta* **1996**, *43*, 1739.

(74) Schwarzenbach, G.; Gut, R.; Anderegg, G. Komplexone XXV. Die polarographische Untersuchung von Austauschgleichgewichten. Neue Daten der Bildungskonstanten von Metallkomplexen der Äthylendiamin-tetraessigsäure und der 1,2-Diaminocyclohexan-tetraessigsäure. *Helv. Chim. Acta* **1954**, *37*, 937.

(75) Baes, C. F., Jr.; Mesmer, R. *The Hydrolysis of Cations*; John Wiley & Sons: New York, 1976.